A highly expressing, soluble, and stable plant-made IgG fusion carrying Zika virus envelope domain III elicits potent immunogenic responses in mice without adjuvant

Andrew G. Diamos*, Mary D. Pardhe, Haiyan Sun, Joseph G. L. Hunter, Jacquelyn Kilbourne, Qiang Chen, and Hugh S. Mason*

Center for Immunotherapy, Vaccines, & Virotherapy, Biodesign Institute at ASU; and School of Life Sciences, Arizona State University, Tempe, AZ 85287

*To whom correspondence should be addressed:

Email: Hugh.Mason@asu.edu; adiamos@asu.edu

Phone: 480-727-8228

Highlights

- Antigen immunogenicity is improved up to 150-fold by fusion to plant-made IgGs.
- High serum IgG endpoint titers >1:500,000 were achieved with only two doses without adjuvant.
- A modified immune complex has high expression, solubility, stability, and immunogenicity.

Summary

While therapeutics based on fusing a protein of interest to the IgG Fc domain have been enormously successful, fewer studies have investigated the vaccine potential of IgG fusions. In this study, we systematically compared the key properties of a panel of plant-made IgG fusion vaccine candidates targeting Zika virus envelope domain III (ZE3). Complement protein C1q binding of the IgG fusions was enhanced by: 1) ZE3 fusion to the IgG N-terminus; 2) removal of the IgG light chain or Fab regions; 3) addition of hexamer-inducing mutations in the IgG Fc; 4) adding a self-binding epitope tag to create recombinant immune complexes (RIC); or 5) producing IgG fusions in plants that lack plant-specific β1,2-linked xylose and α1,3-linked fucose N-linked glycans. We also characterized the expression, solubility, and stability of the IgG fusions. By optimizing the size of polymeric constructs, a potently immunogenic vaccine candidate with improved solubility and high stability was produced at 1.5 milligrams IgG fusion per gram leaf fresh weight (mg/g LFW). In mice, the various IgG fusions elicited high titers of Zika-specific antibodies using only two doses without adjuvant, up to 150-fold higher antibody titers than ZE3 alone. We anticipate these findings will be broadly applicable to the creation of vaccines and antibody-based therapeutics.

Keywords

Zika virus; vaccine; envelope; domain III; IgG fusion; recombinant immune complex; C1q; transient expression; plant-made

Abbreviations

RIC, recombinant immune complex; ZIKV, Zika virus; ZE3, Zika virus envelope domain III; Fc, the C-terminal fragment of crystallization of IgG; Fcγ, Fc from immunoglobulin G; Fab, the antigen-binding fragment of IgG; 6D8, a human IgG1 monoclonal antibody targeting a linear epitope on Ebola virus glycoprotein 1; C1q, the first component of the classical complement pathway; ADCC, antibody-dependent cellular cytotoxicity; CDC, complement dependent cytoctoxicity; FcRn, neonatal Fc receptors.

1. Introduction

Subunit vaccines consisting of recombinant protein antigens are very promising due to their safety, ease of production, and capacity to elicit targeted immune responses directed towards desired epitopes. However, when delivered by themselves, these antigens often fail to generate robust and long-lasting immune responses, necessitating strategies to enhance their immunogenicity (Reed et al., 2013). Protein fusions to the immunoglobulin Fc domain have demonstrated tremendous potential as therapeutic candidates. Fusion of a protein of interest to Fc can enhance the solubility and stability of the fusion partner while also allowing simple and cost-effective purification via protein A/G affinity chromatography (Carter, 2011). Furthermore, by interacting with neonatal Fc receptors (FcRn) in the body, Fc-fusions can escape lysosomal degradation, thereby extending the serum half-life of the Fc-fusion (Roopenian and Akilesh, 2007).

While much of the work with Fc-fusions has focused on improving their therapeutic potential, fewer studies have investigated Fc-fusions as a strategy to enhance the immunogenicity of vaccine antigens. Antigen-presenting cells containing Fcγ receptors and the complement receptor C1q can uptake and process IgG-bound antigen (Bournazos and Ravetch, 2017; Fletcher et al., 2018; Ho et al., 2017). However, these interactions require high avidity binding for activation, and thus monovalent Fc-antigen fusions cannot efficiently utilize these pathways. On the other hand, larger antigen-antibody immune complexes with multivalent Fc domains can cross-link Fc receptors and efficiently bind C1q, resulting in greatly improved uptake and presentation by dendritic cells as well as improved activation of T-cells (Fletcher et al., 2018; Getahun and Heyman, 2006; Ho et al., 2017; van Montfoort et al., 2012). Immune complexes generated by mixing antibody with antigen often yield inconsistent results: immune responses can potentially be directed towards favorable antigenic sites, but overall immunogenicity may not be markedly improved (Hioe et al., 2018; Tsouchnikas et al., 2015). By contrast, recombinant immune complexes (RIC) consisting of an IgG genetically fused to its cognate antigen allow the formation of larger highly immunogenic antigen-antibody clusters that mimic those found during a natural infection. Past research has shown the potential for RIC to produce promising vaccine candidates for *Clostridium tetani* (Chargelegue et al., 2005), Ebola virus (Phoolcharoen et al., 2011a, 2011b), *Mycobacterium tuberculosis* (Pepponi et al., 2014), dengue virus (Kim et al., 2015) and HPV (Diamos et al., 2019).

The glycosylation state of the Fc strongly controls its function and can enhance or inhibit binding to Fcγ receptors, FcRn, and C1q by modulating the stability, conformation, and aggregation of the Fc (Mastrangeli et al., 2019). These alterations result in important differences in antibody effector functions, including antibody-dependent cellular cytotoxicity (ADCC),

antibody-dependent cell-mediated phagocytosis (ADCP), complement-dependent cytotoxicity (CDC), and antibody-dependent enhancement of viral infection (ADE) (Sun et al., 2018). Advances in glycoengineering have allowed targeted optimization of the Fc glycosylation state in a variety of recombinant expression systems (Gupta and Shukla, 2018; Kallolimath and Steinkellner, 2015; Wang et al., 2018). For example, an anti-CD20 antibody produced in glycoengineered plants lacking core xylose and fucose N-linked glycans showed improved binding to FcγRI, FcγRIIIa, and C1q. The antibody also had enhanced ADCC and CDC compared to a commercial anti-CD20 antibody produced in mammalian cells (Marusic et al., 2018). Similarly, anti-DENV antibodies produced in glycoengineered plants have been shown to forgo their ADE activity and, consequently, have superior efficacy and safety profiles than their mammalian cell-produced counterparts (Dent et al., 2016). Antibody therapeutics made in glycoengineered plants have been used to treat rhesus macaques and humans with Ebola (Lyon et al., 2014; Olinger et al., 2012; Qiu et al., 2014; Zeitlin et al., 2011), HIV (Forthal et al., 2010), and Chikungunya virus disease (Hurtado et al., 2019).

Several mutations in the Fc region that confer desirable properties to antibodies have been identified. Introduction of M252Y, S254T, and T256E mutations increased the serum half-life of an anti-respiratory syncytial virus antibody from 20 days to 60 days in humans by improving interactions with FcRn under low pH conditions (Robbie et al., 2013). An H237Y mutation reduced detrimental cleavage of the hinge region while improving FcγRIII binding and ADCC activity (Yan et al., 2012). Engineering additional disulfide bonds has also been reported to prevent unfolding and aggregation of Fc-fusions (Zeng et al., 2018). For example, S239D and I332E mutations improved FcγRIII binding and ADCC activity of a CD37 antibody (Heider et al., 2011; Lazar et al., 2006). Replacing the IgG1 hinge region with the

longer hinge region from IgG3 or from a camelid antibody increased ADCC of an epidermal growth factor receptor antibody (D'Eall et al., 2019), while an IgG1 with E345R, E430G, and S440Y mutations formed hexamers that had greatly enhanced C1q binding and complement activation (Diebolder et al., 2014). The mutations T437R and K248E also promoted multimerization and improved effector functions of an OX40 receptor antibody (Zhang et al., 2017).

Building on these recent advances in understanding the immunogenicity of Fc-fusions, we designed a panel of IgG fusions as vaccine candidates for Zika virus (ZIKV). Previous work has shown that antibodies can be properly assembled with human-like glycosylation (Strasser et al., 2008) and expressed at very high levels in plants (Diamos et al., 2016, 2020a). In this study, we expressed, characterized, and evaluated the immunogenicity of ZIKV envelope domain IIII (ZE3) fused to a variety of IgG1 variants in glycoengineered *Nicotiana benthamiana*. A highly expressing and highly stable IgG fusion was identified that induced potent and neutralizing immunity to ZIKV in only two doses without adjuvant.

2. Results

2.1 Modified IgG fusions displaying ZIKV envelope domain III strongly bind complement receptor C1q

ZE3 is a promising subunit vaccine candidate, however, it is not strongly immunogenic on its own, necessitating high antigen doses with adjuvant and repeated immunizations (Yang et al., 2017). In this study, we designed a panel of human IgG1 variants based on the previously characterized humanized anti-Ebola monoclonal antibody 6D8 (Phoolcharoen et al., 2011a) fused to ZE3 (**Fig. 1A**). A RIC construct was created by fusing epitope-tagged ZE3 via a flexible linker to the C-terminus of the 6D8 heavy chain (Mason, 2016). The construct is referred to as

"HLZe" as it contains the **H**eavy chain, **L**ight chain, C-terminal **Z**E3 fusion, and **e**pitope tag. As a control for immune complex formation, an otherwise identical construct was created without the epitope tag (construct "HLZ") and thus would not be expected to form immune complexes. The 6D8 antibody without any modification or fusions is referred to as construct "HL." First, to evaluate complex formation, we investigated binding of the IgG fusion constructs to complement receptor C1q, which requires polymeric IgG for efficient binding. C1q mediates immune complex uptake into antigen presenting cells, and complement-coated immune complexes play a key role in activating and maintaining long-term immunity (Croix et al., 1996; McCloskey et al., 2011; Phan et al., 2007; West et al., 2018). To improve C1q binding, all constructs were expressed in glycoengineered *Nicotiana benthamiana* that have suppressed fucosyl- and xylosyl transferase activities (Kallolimath and Steinkellner, 2015). HL or RIC made in glycoengineered plants showed highly improved C1q binding compared to constructs expressed in wildtype plants (**Fig. S1**). RIC are thought to engage C1q with high avidity due to densely clustered antigen-antibody complexes and, as expected, HLZe showed greatly improved C1q binding compared to HLZ ($p < 0.001$) (**Fig. 1B**). A small increase in C1q binding was also noted with HLZ compared to HL ($p < 0.05$) (**Fig. 1B**), suggesting low-level aggregation of the construct or slight alteration of Fc conformation.

It has been suggested that the antibody Fab arms play a regulatory role in complement activation by inhibiting C1q binding unless cognate antigens are bound by the antibody (Wang et al., 2016). In agreement with these data, we find that the addition of soluble antigen carrying the 6D8 epitope tag improved C1q binding (**Fig. S2**, compare HL vs HL + Ag). In addition, C1q binding was greatly enhanced either by removal of the antibody light chain or, interestingly, by antigen fusion to the heavy chain N-terminus (**Fig. S2**, compare HL, H, and ZHL). Therefore, we

created a construct with ZE3 fused to the N-terminus of the heavy chain (construct "ZH") in the absence of the light chain, and found it to efficiently bind C1q (**Fig. 1B**). To further improve interaction with C1q, we made a construct that was identical to ZH except for mutations E345R, E430G, and S440Y in the Fc region, which favor formation of hexamers (Diebolder et al., 2014). This construct (ZHx) further improved C1q binding compared to ZH ($p < 0.001$) (**Fig. 1B**). Past studies have shown that IgG1 Fc fusions (lacking VH and CH1 domains) produce variable levels of C1q binding depending on the fusion partner (Lagassé et al., 2019) (Zhang et al., 2019). ZE3 N-terminally fused to the 6D8 Fc (**Fig. 1A** construct "ZFc") showed very strong C1q binding (**Fig. 1B**). We constructed a simplified RIC that also lacked the light chain constant region, such that the variable light (VL) domain of 6D8 was inserted between the variable heavy (VH) and CH1 domains of 6D8, yielding construct "HVL". This construct bound antigen tagged with the 6D8 epitope, albeit at a somewhat reduced level compared to unaltered 6D8 (**Fig. S3**). This single-chain Fab configuration was fused to Ze to create the single chain RIC HVLZe (**Fig. 1A**), which displayed strong C1q binding (**Fig. 1B**).

2.2 Reducing RIC self-binding improves solubility without reducing C1q binding

RIC suffer from low yield of soluble product (Diamos et al., 2019). Addition of the 6D8 epitope tag to the C-terminus of HL renders the antibody mostly insoluble, however this is prevented by removal of the light chain, which is needed for epitope binding (Kim et al., 2015), suggesting that the insolubility arises from large complexes of antibody bound to the epitope tag (**Fig. S4**). To improve RIC solubility, we shortened the 6D8 epitope tag in order to reduce antibody binding. Reducing the epitope tag on HLZe to the minimal reported binding region for 6D8 (Wilson et al., 2000) (construct "HLa," epitope sequence VYKLDISEA) showed no improvement in solubility, nor did removal of a single amino acid from the C-terminus

(construct "HLb," VYKLDISE) (**Fig. S5A**). However, further removal of a single amino acid from the N-terminus (construct "HLc," YKLDISE), and additional truncation in construct "HLd" (YKLDIS) resulted in greatly improved solubility (**Fig. S5B**). Thus, HLd was introduced to HLZe (construct HLZd) and characterized. Despite reducing epitope binding by approximately 25-fold by ELISA (**Fig. S5C**), HLZd still maintained very strong C1q binding (**Fig. 1B**), while the otherwise identical construct HLZ, which lacks an epitope tag, had 10-fold lower C1q binding (**Fig. 1B**). These data suggest that some complex formation was still mediated by the truncated epitope tag.

2.3 High expression of IgG fusions in plants

To measure the yield of fully assembled IgG fusions, an ELISA assay was employed that first captured ZE3 and then detected human IgG, using purified and quantified HLZ as a standard. To detect any proteolytic cleavage of ZE3, an ELISA measuring only total IgG was also used as a comparison, using purified and quantified unfused HL antibody as standard. When soluble fractions were probed for the presence of both ZE3 and IgG, the highly soluble monomeric construct ZH yielded 0.83 mg fully formed product per gram leaf fresh weight (mg/g LFW), and the similar ZFc yielded 0.58 mg/g LFW (**Fig. 2A**). However, when measuring the total IgG content, the yield of ZH was roughly 20% higher and, for ZFc, 2.5-fold higher than ZE3 ELISA, which suggests that ZH and especially ZFc are susceptible to proteolytic cleavage. This finding was confirmed by visualization of the ZFc cleavage products on SDS-PAGE (**Fig. 2B**). HLZ accumulated only 0.17 mg/g LFW fully assembled product, with roughly 40% ZE3 lost to cleavage, suggesting general instability of the construct (**Fig. 2A, 2B**). By ELISA, the polymeric RIC constructs seemingly had lower yields than the monomeric constructs: HLZe and HLZd only accumulated 0.04 mg/g LFW and 0.30 mg/g LFW respectively, and the hexameric ZHx

accumulated only 0.08 mg/g LFW (**Fig. 2A**). However, when visualized under reducing SDS-PAGE conditions, HLZd was the highest expressing construct, accumulating an estimated 1.5 mg/g LFW (**Fig. 2A, 2B**). This discrepancy likely arises due to complexed HLZd being inaccessible to the antibody probe by ELISA. Importantly, the gel quantification results agreed with the ELISA results for all the monomeric constructs, but not for any of the polymeric constructs (**Fig. 2A**). Therefore, the polymeric constructs can only be accurately quantified after breaking them apart with SDS-PAGE buffer. Thus, the total yield of HLZe and ZHx was also higher when measured by gel quantification (**Fig. 2A, 2B**). Construct HVLZe yielded only 0.02 mg/g LFW soluble product by ELISA and was not visible by SDS-PAGE (**Fig. 2A**), although we detected very high levels when extracting with 7.5 M urea (data not shown), suggesting insolubility resulted in the low yield.

2.4 Purification and aggregation of IgG fusion constructs

IgG fusions were purified to >95% homogeneity using a simple one-step purification via protein G affinity chromatography. In agreement with the expression data, the more polymeric constructs showed less degradation than the other constructs, and the ZFc fusion had particularly high levels of degradation (**Fig. 3**). To investigate the aggregation characteristics of each construct, purified IgG fusions were analyzed by sucrose gradient sedimentation. Consistent with the formation of large immune complexes, HLZe and HVLZe were found mostly in the bottom of the gradient while HLZ, ZH, and ZFc were found mostly at the top of the gradient (**Fig. 4A, 4B**). Soluble extracts of ZHx contained both low-density material as well as some very high-density material (**Fig. 4B**). Extracts of HLZd showed intermediate density compared to HLZ and HLZe (**Fig. 4A**) which, when taken together with the expression data and C1q binding, are consistent with HLZd forming smaller, more soluble immune complexes compared to HLZe.

2.5 Polymeric constructs have improved stability

The stability of each construct was analyzed by comparing fully formed products and degradation products on SDS-PAGE gels after treatment with various temperature conditions. The initial level of degradation, which corresponds to any degradation that occurred during expression, purification, or the initial freeze/thaw, was substantially reduced (20-40% more fully formed product) in polymeric constructs, compared to monomeric constructs (**Fig. 5A**). After five freeze-thaw cycles or two weeks at 4°C, small amounts of degradation (2-5%) were observed with all constructs (**Fig. 5A**). High concentrations (>1 mg/ml) of HLZe and HVLZe precipitated after several days at 4°C (data not shown), probably due to the formation of very large insoluble complexes, highlighting the undesirability of these constructs. At room temperature, most constructs had 10-15% degradation after two weeks (**Fig. 5A**). Overall, the polymeric constructs retained the highest stability, while the monomeric constructs, and especially the Fc fusion, degraded more rapidly (**Fig. 5A**). Most constructs retained strong C1q binding after storage; however, after room temperature storage or repeated freeze-thaw cycles, but not 4°C storage, construct HLZ displayed increased C1q binding (**Fig. 5B**). This may be due to aggregation, degradation of the Fab regions, or loss of light chain, as degradation products are visible on SDS-PAGE (**Fig. 3**). Conversely, construct ZFc lost C1q binding ability as it became more degraded, especially after freeze-thaw cycles, possibly due to degradation of the C1q binding regions (**Fig. 5B**). Taken together with the expression data, constructs with intermediate levels of self-binding (e.g. HLZd and ZHx) showed the highest stability during both extraction and storage, while maintaining high solubility.

2.6 IgG fusion enhances ZE3 immunogenicity

Due to their improved binding of C1q and uptake via Fc receptors on antigen presenting cells, IgG fusions have enhanced immunological properties (Czajkowsky et al., 2012). To investigate the immunogenicity of the IgG fusions created here, BALB/c mice (n = 6) were immunized subcutaneously, without adjuvant, with two doses of each IgG fusion construct such that each dose of ZE3 delivered was 8 μg. As a control, mice were also immunized with 8 μg His-tagged plant-expressed ZE3. As expected, all IgG fusions very strongly enhanced the production of ZE3-specific IgG, producing 20-fold to 150-fold higher total IgG titers than ZE3 alone (**Fig. 6A**, $p < 0.01$ compared to ZE3). The level of IgG2a antibodies were also measured because they have important antiviral effector functions (Lu et al., 2018) and are correlated with T-cell activation (Huber et al., 2006) and complement activity (West et al., 2018). All IgG fusions significantly enhanced the production of IgG2a compared to ZE3 alone (**Fig. 6B**, $p < 0.01$ compared to ZE3). The construct HLZ, which displayed the lowest C1q binding (**Fig. 1B**), had a significantly reduced production of IgG2a compared to most other fusions (**Fig. 6B**, $p < 0.05$ compared to HLZ). Sera from mice immunized with all IgG fusions were potently neutralizing and reached a 50% neutralization titer >1:10 (**Fig 7,** $p < 0.0001$ compared to sera from PBS-injected mice). All IgG fusions also elicited significantly higher neutralizing responses than His-tagged ZE3 (**Fig 7,** $p < 0.024$ compared to ZE3).

3. Discussion

Previous work has shown that several IgG fusion strategies have potential to enhance antigen immunogenicity (Kim et al., 2018; Konduru et al., 2011; Loureiro et al., 2011; Webster et al., 2018; Zhao et al., 2018), however the key characteristics to produce an optimal vaccine candidate have not been directly compared. In this study, we systematically evaluated seven

different IgG fusion constructs to determine which factors affect expression, stability, solubility, and immunogenicity. Compared to His-tagged ZE3 antigen, many of the best IgG fusion groups produced over 100-fold higher antibody responses, supporting the use of IgG fusions as a general method to improve antigen immunogenicity. Overall, construct HLZd had nearly double the yield of the next closest construct (**Fig. 2**) while maintaining high stability (**Fig. 5**), solubility (**Fig. S5B**), and immunological properties (**Figs. 6, 7**). The overall properties of each construct are summarized in Table 1. These findings warrant further development of HLZd as a vaccine candidate, and we anticipate these findings will be broadly applicable to the development of IgG fusion vaccines targeting other pathogens.

Though potently immunogenic, traditional RIC may be undesirable for several reasons. First, the large complex size renders them poorly soluble upon extraction (**Figs. 2A/S2** and Diamos *et al.*, 2019) and concentrations above 1-2 mg/ml cause precipitation during storage (data not shown). Second, very large RIC may be too big to efficiently drain to lymph nodes from the injection site, which favor particles <200 nm (Manolova et al. 2008). Indeed, hexamer-sized IgG may be the optimal substrate for efficient C1q binding (Diebolder et al., 2014; Wang et al., 2016). Therefore, we reduced the binding affinity of the RIC by mutating the 6D8 epitope tag (construct HLZd). Notably, compared to traditional RIC, HLZd was significantly more soluble (**Fig. S5B**), allowing recovery of very high levels of fully formed product (1.5 mg/g LFW) (**Fig. 2A**).

While high affinity Fc receptors such as FcγRI/CD64 may interact with monomeric Fc, low affinity receptors such as FcγRII/CD32 and FcγRIII/CD16, as well as complement receptor C1q, require polymeric Fc for efficient binding (Bournazos and Ravetch, 2017; Diebolder et al., 2014). For instance, a polymeric dengue IgG fusion vaccine showed enhanced immunogenicity

in human adenotonsillar tissue compared to a monomeric form of the same IgG fusion; however, both polymeric and monomeric forms showed equivalent immunogenicity in mice expressing human FcγRI/CD64 (Kim et al., 2018). In agreement with the results of Kim et al., the theoretically monomeric construct HLZ (consisting of ZE3 fused to the C-terminus of HL without any epitope tag) still elicited high IgG titers (**Fig. 6A**), suggesting binding high affinity Fc receptors may be sufficient for strong B-cell activation. Additionally, while human antibodies have recently been shown to have similar binding affinities to mouse Fc receptors compared to mouse antibodies, human IgG1 has somewhat reduced binding to low affinity mouse FcγRIII/CD16 (Dekkers et al., 2017), which may have further reduced the immunogenic differences between polymeric and monomeric constructs observed in these assays. However, despite similar total IgG titers, IgG2a titers were significantly reduced for HLZ compared to the polymeric constructs (**Fig. 6B**). As IgG2a is a general indicator of a Th1 response (Huber et al., 2006) and complement activation is involved in T-cell immunity (West et al., 2018), HLZ may have reduced T-cell activation compared to more polymeric constructs. This is important because T-cell activation and complement activation are important for the generation of long-term B-cell immunity (Akkaya et al., 2020; West et al., 2018). Further investigation of T-cell immunity is needed to better compare the immunological characteristics of these constructs.

Antigen binding may induce conformational changes in an antibody, resulting in improved hexamer formation and subsequently improved C1q binding (Wang et al., 2016). Mixing 6D8 with an antigen containing the 6D8 epitope produced only a small increase in C1q binding (**Fig. S2**). However, antigen fusion to the 6D8 N-terminus had a more pronounced effect on C1q binding (**Fig. 1**), perhaps by strongly inducing conformational changes similar to antigen binding which allow hexamer formation (Diebolder et al., 2014). In general, we have found that

antigen fusion to the 6D8 N-terminus greatly enhances C1q binding for a variety of large and small antigens (data not shown). Furthermore, removal of the 6D8 light chain (construct ZH) also substantially enhanced C1q binding (**Fig. 1**). These findings agree with the hypothesis that the Fab portions of the antibody plays a regulatory role in C1q binding. Additionally, removal of the light chain may also impact glycosylation and thus C1q binding (He et al., 2014). While construct ZHx contains hexamer-inducing mutations (Diebolder et al., 2014; Wang et al., 2016), C1q binding was already enhanced via N-terminal ZE3 fusion and removal of the light chain, obscuring benefits from these mutations. Despite its strong immunogenicity, ZHx had reduced yield compared to ZH (**Fig. 2**). Additionally, ZHx appeared to have some large material found in the very bottom of the sucrose gradients that was not found in construct ZH (**Fig. 4**), suggesting the hexamer-inducing mutations may contribute to the formation of larger aggregates.

Interestingly, construct HLZ produced a small but repeatable improvement in C1q binding (**Fig. 1B**). This may suggest some low-level aggregation due to the ZE3 fusion (**Fig. 4A**, compare HL and HLZ). The expression of HLZ was generally low, suggesting C-terminal ZE3 fusion may interfere with folding or otherwise cause instability (**Fig. 2A**). Many degradation products are visible by SDS-PAGE following purification (**Fig. 3**) and interestingly the C1q binding of HLZ continued to increase upon further degradation by incubation for 2 weeks at RT or repeated freeze-thaw cycles (**Fig. 5B**). These data suggest that the degradation products may be more highly immunogenic than the original construct, as light chain removal strongly improves C1q binding (**Fig. S2**). This finding may have also contributed to the relatively high immunogenicity produced by HLZ (**Fig. 6A**). By contrast, the polymeric constructs, especially HLZd and ZHx (**Fig. 4**), were more stable both prior to and during extraction, as well as upon storage (**Fig. 5A**). Consistent with their inaccessibility to antibody probes during ELISA (**Fig.**

329 **2A**), the intramolecular and intermolecular associations of these constructs may protect them
330 from proteolysis or other degradative processes.

331 N-terminal ZE3 fusion to the 6D8 CH2 domain (construct ZFc) greatly improved C1q
332 binding (**Fig. 1**), elicited very high antibody titers (**Fig. 6**) and potently neutralized ZIKV (**Fig.**
333 **7**). While most current antibody fusion vaccines use constructs similar to ZFc, many properties
334 of Fc fusions, including C1q binding, vary based on the individual fusion partner and thus must
335 be determined empirically for each fusion (Lagassé et al., 2019). Interestingly, some Fc fusion
336 constructs form hexamers (Zhang et al., 2019), which may explain the strong immunogenicity of
337 ZFc observed here. Studies that can more specifically characterize the oligomeric status of ZFc
338 are needed to further address these questions. Despite its strong immunogenicity, ZFc was
339 remarkably unstable: ~50% of the ZE3 was cleaved off either before or during extraction (**Fig.**
340 **2A**, **2B**) even when directly extracted in SDS sample buffer or with protease inhibitors (data not
341 shown), and less than 25% of full-size ZFc molecules remained intact upon repeated freeze-thaw
342 or storage (**Fig. 5A**). Unlike HLZ, this degradation was associated with a loss in C1q binding
343 (**Fig. 5B**), probably due to impairment of the Fc receptor binding domains. These data suggest
344 ZFc may perform less well if stored even for short periods of time prior to immunization, thus
345 limiting its use as a vaccine candidate. ZFc has fewer disulfide bonds than whole IgG, and in
346 general Fc fusions often suffer from instability or undesirable aggregation (Zeng et al., 2018).
347 Further protein engineering, including optimization of linkers, could likely improve the stability
348 and expression of these constructs. While ZFc elicited high titers, to deliver 8 μg ZE3
349 (discounting the weight of the IgG fusion partner), the total amount of purified sample used for
350 immunization had to be nearly tripled to account for the high degradation and resulting loss of
351 the ZE3 fusion. Whether this increased delivery of unfused Fc as well as other possible

352 degradation products may have contributed to the high immunogenicity observed in this study is
353 unknown.

354 While traditional RIC require coexpression of both the heavy and light chains, this can be
355 simplified by creating a single chain antibody with the variable light domain fused to the variable
356 heavy domain. Therefore, we created HVLZe, which had higher C1q binding than traditional
357 RIC **(Fig. 1B)** and equivalently high stability at the tested conditions **(Fig. 5A).** Since this single
358 chain configuration reduced binding to the epitope tag when compared with the full 6D8
359 antibody (HL), we expected that the HVLZe would form smaller complexes, which agrees with
360 our sucrose gradient data showing reduced sedimentation compared to HLZe (**Fig. 4A**). However,
361 some very dense material remained, unlike with construct HLZd, which probably indicates
362 aggregation that may have contributed to the low expression of HVLZe (**Fig. 2**). Likely, further
363 reducing the epitope binding of HVLZe would improve its solubility.

364 In summary, we have developed a cheap, fast, and efficient plant expression system to
365 produce and purify high levels of IgG fusion vaccine candidates for ZIKV. Plant recombinant
366 expression systems are particularly well suited to make IgG fusions vaccines, like the ones
367 described in this study, since they have inherent safety, high scalability, and low production costs
368 when compared to mammalian cell systems (Alam et al., 2018; Buyel, 2019; Chen and Davis,
369 2016; Gleba et al., 2014). These benefits can be of special value for vaccine production in
370 developing countries (Ma et al., 2013). In addition to their widespread therapeutic value, IgG
371 fusions are promising vaccine candidates due to their safety and self-adjuvating nature
372 (Czajkowsky et al., 2012; Webster et al., 2018). Notably, the IgG fusions were potently
373 immunogenic and reached the threshold of protective neutralizing antibody titers (>10) (Yang et
374 al., 2017) after only two doses in the absence of adjuvant, demonstrating the excellent potential

of plant-made IgG fusion vaccines. By directly comparing many different IgG fusion strategies, we have identified construct HLZd that is highly expressing, stable, soluble, and immunogenic. These studies warrant future research in animal models, and we anticipate our findings will be broadly applicable to other vaccine antigens or antibody-based therapeutics.

4. Experimental Procedures

4.1 Vector Construction

The construction of a geminiviral replicon plant expression vector for ZE3, as well as its fusion to the 6D8 C-terminus (pBYR11eM-h6D8ZE3, referred to here as construct “HLZe”) or N-terminus with epitope tag (pBYR11eMa-BAZE3-Hgp371) or without epitope tag (pBYR11eMa-BAZE3-H) have been previously described (Diamos et al., 2020b, 2020a) A vector pBYKEMd2-6D8 expressing the full 6D8 mAb without ZE3 fusion (construct “HL”) has been previously described (Diamos et al., 2020b, 2020a). To create a vector expressing only the light chain of 6D8, pBYKEMd2-6D8 was digested with XhoI and the vector was self-ligated to yield pBYKEMd-6D8K. A vector expressing only the heavy chain of 6D8 (construct “H”) was created by digesting pBYKEMd2-6D8 with SacI and self-ligating the vector, to yield pBYKEMd-6D8H. The 6D8 epitope binding tag was added to pBYKEMd-6D8H by digesting pBYR11eMa-BAZE3-Hgp371 with BsaI-SacI and inserting the tag-containing fragment into pBYKEMd-6D8H digested with BsaI-SacI, yielding pBYKEMd-6D8Hgp371 (construct “HLe” when coexpressed with light chain). To remove the epitope tag from HLZe, pBYR11eM-h6D8ZE3 was digested with BamHI-SacI and ligated with a fragment containing ZE3 obtained via amplification with primers ZE3-Bam-F (5’-gcgggatccaagggcgtgtcatactcc) and ZE3-Sac-R (5’-acagagctcttaagtgctaccactcctgtg) and subsequent digestion with BamHI-SacI. The resulting vector, pBYKEMd-HZE3, was coinfiltrated with pBYKEMd-6D8K to produce construct “HLZ.”

To produce ZE3 fused to the 6D8 N-terminus without light chain, pBYR11eMa-BAZE3-H was digested with SacI and the vector vector was self-ligated, yielding pBYKEMd-ZE3H (construct "ZH"). To introduce hexamer mutations, a region of the 6D8 heavy chain constant region was synthesized (Integrated DNA Technologies, Iowa, USA) containing the E345R, E430G, and S440Y mutations, then digested with BsaI-SacI and used to replace the BsaI-SacI region of 6D8 in pBYKEMd-ZE3H, yielding pBYKEMd-ZE3Hx (construct "ZHx"). RIC epitope tag mutant "a" was generated by annealing oligos 6D89-F (5'-ctagtgtttacaagctggacatatctgaggcataagagct) and 6D89-R (5'- cttatgcctcagatatgtccagcttgtaaaca) and ligating them into pBYR11eM-h6D8ZE3 digested SpeI-SacI; mutant "b" was generated by first amplifying mutant "a" with primers gpDISE-Sac-R: (5'-tttgagctcttactcagatatgtccagcttgtaaac) and 35S-F (5'aatcccactatccttcgc), then digesting the product with SpeI-SacI and ligating it into pBYR11eM-h6D8ZE3 digested with SpeI-SacI. Mutants "c" and "d" were created similarly to mutant "a" using overlapping oligos 6D87-F (5'-ctagttacaagctggacatatctgagtaagagct) and 6D87-R (5'-cttactcagatatgtccagcttgtaa) for "c" and 6D86-F (5'-ctagttacaagctggacatatcttaagagct) and 6D86-R (5'-cttaagatatgtccagcttgtaa).

In order to make a construct in which the variable heavy (VH) domain is linked to a variable light chain (VL) domain that, in turn, is directly fused to the constant region of the 6D8 antibody, the variable regions were first obtained through PCR amplification and end-tailoring of segments from pBYR11eM-h6D8ZE3. For the VH domain, the primers LIR-H3A (5'-aagcttgttgttgtgactccgag) and 6D8VH-Spe-R (5'- cggactagtagctgaagacactgtgac) were used. The VL region was obtained through PCR amplification of pBYR11eM-h6D8ZE3 with primers 35S-F (5'-aatcccactatccttcgc) and 6D8VK-Nhe-R (5'-cgtgctagccttgatctccactttggtc). In order to fuse VL region to the constant region of a human IgG antibody, a subclone was created by digesting the PCR fragment with XhoI-NheI and inserting it into a vector, pKS-HH-gp371, that contained

the 6D8 heavy chain (Kim et al., 2015). This subclone was named pKS-VL. Next, pBYKEM-6D8K was digested with SbfI-SacI, the PCR product that amplified the variable heavy chain fragment was digested SbfI-SpeI, and the variable light chain subclone was digested SpeI-SacI. These fragments were assembled to create pBYKEMd2-VHLVK (construct "HVL"). Finally, this construct was used to create pBYKEMd2-HVLZe by a two-fragment ligation. The pBYKEMd2-VHLVK construct was digested BsaI and SacI to obtain the vector fragment along with the variable regions of the heavy and light chains. To obtain the ZE3 antigen segment and the epitope tag, pBYR11eM-h6D8ZE3 was also digested BsaI-SacI. The resulting construct, which was used to produce HVLZe, was named pBYKEMd-HVLZe.

4.2 Agroinfiltration of *Nicotiana benthamiana* Leaves

Binary vectors were separately introduced into *Agrobacterium tumefaciens* EHA105 by electroporation. The resulting strains were verified by restriction digestion or PCR, grown overnight at 30°C, and used to infiltrate leaves of 5- to 6-week-old *N. benthamiana* maintained at 23-25°C. Briefly, the bacteria were pelleted by centrifugation for 5 min at 5,000g and then resuspended in infiltration buffer (10 mM 2-(N-morpholino)ethanesulfonic acid (MES), pH 5.5 and 10 mM MgSO4) to OD600=0.2, unless otherwise described. The resulting bacterial suspensions were injected by using a syringe without needle into leaves through a small puncture (Huang and Mason, 2004). To evaluate the effects of glycosylation, transgenic plants silenced for xylosyltransferase and fucosyltransferase were employed (Castilho and Steinkellner, 2012). Plant tissue was harvested at 5 days post infiltration (DPI).

4.3 Protein Extraction and Purification

Crude protein was extracted by homogenizing agroinfiltrated leaf samples with 1:5 (*w:v*) ice cold extraction buffer (25mM Tris-HCl, pH 8.0, 125mM NaCl, 3mM EDTA, 0.1% Triton X-100, 10 mg/mL sodium ascorbate, 0.3 mg/mL phenylmethylsulfonyl fluoride) using a Bullet Blender machine (Next Advance, Averill Park, NY) following the manufacturer's instruction. Homogenized tissue was rotated at 4°C for 30 min. The crude plant extract was clarified by centrifugation at 13,000*g* for 15 min at 4°C and the supernatant was analyzed by SDS-PAGE or ELISA. Alternatively, to evaluate solubility of proteins in the original homogenate, the pellet was designated the insoluble fraction and treated with SDS sample buffer at 100˚C for 10 min before loading on SDS-PAGE.

IgG variants were purified by protein G affinity chromatography. Agroinfiltrated leaves were blended with 1:3 (w:v) ice cold extraction buffer (25mM Tris-HCl, pH 8.0, 125mM NaCl, 3mM EDTA, 0.1% Triton X-100, 10 mg/mL sodium ascorbate, 0.3 mg/mL phenylmethylsulfonyl fluoride), stirred for 30 min at 4°C, and filtered through miracloth. To precipitate endogenous plant proteins, the pH was lowered to 4.5 with 1M phosphoric acid for 5 min while stirring, then raised to 7.6 with 2M Tris base. Following centrifugation for 20 min at 16,000*g*, the clarified extract was loaded onto a Protein G column (Thermo Fisher Scientific, Waltham, MA, USA) following the manufacturer's instructions. Purified proteins were eluted with 100mM glycine, pH 2.5, directly into collection tubes containing 1M Tris-HCl pH 8.0 to neutralize the elution buffer, and stored at -80˚C.

ZE3-His expressed from pBYe3R2K2Mc-BAZE3 was purified by metal affinity chromatography. Protein was extracted as described above, but without acid precipitation. The clarified extract was loaded onto a column containing TALON Metal Affinity Resin (BD

Clontech, Mountain View, CA) according to the manufacturer's instructions. The column was washed with PBS and eluted with elution buffer (PBS, 150mM imidazole, pH 7.4). Peak ZE3 elutions were pooled, dialyzed against PBS, and stored at -80˚C.

4.5 SDS-PAGE and Western Blot

Plant protein extracts or purified protein samples were mixed with SDS sample buffer (50 mM Tris-HCl, pH 6.8, 2% SDS, 10% glycerol, 0.02 % bromophenol blue) and separated on 4-15% stain-free polyacrylamide gels (Bio-Rad, Hercules, CA, USA). For reducing conditions, 0.5M DTT was added, and the samples were boiled for 10 min prior to loading. Polyacrylamide gels were visualized and imaged under UV light, then transferred to a PVDF membrane. For IgG detection, the protein transferred membranes were blocked with 5% dry milk in PBST (PBS with 0.05% tween-20) overnight at 4°C and probed with goat anti-human IgG-HRP (Sigma-Aldrich, St. Louis, MO, USA diluted 1:5000 in 1% PBSTM). Bound antibody was detected with ECL reagent (Amersham, Little Chalfont, United Kingdom).

4.6 C1q Binding

96-well high-binding polystyrene plates (Corning Inc, Corning, NY, USA) were coated with 15 µg/ml human complement C1q (PFA, MilliporeSigma, MA) in PBS for 2h at 37°C. The plates were washed 3 times with PBST, and then blocked with 5% dry milk in PBST for 15 minutes. After washing 3 times with PBST, purified human IgG (Southern Biotech, Birmingham, AL, USA) and purified IgG-ZE3 fusions were added at 0.1 mg/ml with 10-fold serial dilutions and incubated for 1.5 hours at 37°C. After washing 3 times with PBST, bound IgG was detected by incubating with 1:1000 polyclonal goat anti human IgG-HRP (Southern Biotech, Birmingham, AL, USA) for 1h at 37°C. The plates were washed 4 times with PBST, developed with TMB

487 substrate (Thermo Fisher Scientific, Waltham, MA, USA), stopped with 1M HCl, and the
488 absorbance was read at 450nm.

489 **4.7 6D8 Epitope Binding**

490 To test the ability of HVL to bind to the 6D8 epitope tag, 900 ng of purified dengue
491 consensus envelope domain III tagged with 6D8 epitope (Kim et al., 2015) were bound to a 96-
492 well high-binding polystyrene plate (Corning Inc, Corning, NY, USA). After a 1-hour incubation
493 at 37°C, the plate was washed thrice with PBST and blocked with 5% dry milk in PBST for 30
494 minutes. Then, the plate was washed thrice with PBST and various dilutions of either purified
495 HLV or full-length 6D8 antibody were added to the plate. The plate was incubated at 37°C for 1-
496 hour, washed thrice with PBST and detected with HRP-conjugated mouse anti-human IgG (Fc
497 only) (Southern Biotech, Birmingham, AL, USA) antibody at a 1:2000 dilution. Then, the plate
498 was thoroughly washed with PBST and developed with TMB substrate (Thermo Fisher Scientific,
499 Waltham, MA, USA). The absorbance was read at 450nm.

500 **4.8 Sucrose gradient density centrifugation**

501 Purified samples of each IgG fusion (100 µl) were loaded onto discontinuous sucrose
502 gradients consisting of 350 µl layers of 5, 10, 15, 20, and 25% sucrose in PBS in a 2.0 ml
503 microcentrifuge tubes and centrifuged at 21,000*g* for 16□h at 4□°C. Fractions were collected
504 from the top and analyzed by SDS-PAGE, followed by visualization on stain-free gels (Bio-Rad,
505 Hercules, CA, USA). The relative band intensity of each fraction was determined using ImageJ
506 software, with the peak band arbitrarily assigned the value of 1.

507 **4.9 Stability of IgG fusions during storage**

508 After purification, samples of purified IgG fusions were frozen at -80˚C. Samples were
509 either untreated (referred to as “initial”), or thawed and then subjected to either five additional

freeze/thaw cycles, or incubated for 2 weeks at 4°C, or incubated for 2 weeks at 23˚C. Initial and treated samples were visually inspected for any signs of precipitation, and then analyzed by reducing and non-reducing SDS-PAGE to observe cleavage of ZE3 or other degradation products. ImageJ analysis was used to compare the band intensity of the fully formed product to that of any degradation products. Each sample was also analyzed as described in section 4.6 for C1q binding.

4.10 Immunization of mice and sample collection

All animals were handled in accordance to the Animal Welfare Act and Arizona State University IACUC. Female BALB/C mice, 6-8 weeks old, were immunized subcutaneously with purified IgG fusion variants. In all treatment groups, the total weight of antigen was set to deliver an equivalent 8 µg of ZE3. Doses were given on days 0 and 14. Serum collection was done as described (Santi et al., 2008) by submandibular bleed on days 0, 14, and 28.

4.11 Antibody Measurements

Mouse antibody titers were measured by ELISA. Plant-expressed 6-His tagged ZE3 at 50 ng/well was bound to 96-well high-binding polystyrene plates (Corning Inc, Corning, NY, USA), and the plates were blocked with 5% nonfat dry milk in PBST. After washing the wells with PBST (PBS with 0.05% Tween 20), the mouse sera were diluted with 1% PBSTM (PBST with 1% nonfat dry milk) and incubated. Mouse antibodies were detected by incubation with polyclonal goat anti-mouse IgG-horseradish peroxidase conjugate (Sigma-Aldrich, St. Louis, MO, USA). The plate was developed with TMB substrate (Thermo Fisher Scientific, Waltham, MA, USA), stopped with 1M HCl, and the absorbance was read at 450nm. Endpoint titers were taken as the reciprocal of the lowest dilution which produced an OD_{450} reading twice the background produced using PBS as the sample. IgG2a antibodies were measured from sera

diluted 1:100 in 1% PBSTM and detected with IgG2a horseradish peroxidase conjugate (Santa Cruz Biotechnology, Dallas, TX, USA).

4.12 Plaque Reduction Neutralization Assay

Serum samples from terminal blood collection were pooled for each mouse group and heat inactivated. As described previously (Dent et al., 2016), the PRNT assay was carried out using mouse sera diluted in Opti-Mem media (Invitrogen) at ratio of 1:10. Each sample was incubated with 100 pfu ZIKV (PRVABC59, ATCC# VR-1843) in equal volume for 1hr at 37°C before the virus/serum mixture was added to each well of VERO cells (ATCC # CCL-81) in a 24 well plate. The virus/serum mixture was aspirated after a 1.5 hour incubation at 37°C. Subsequently, VERO cells were overlaid with 0.8% agarose in DMEM medium containing 5% FBS (Invitrogen, CA) and incubated at 37°C for three days. Finally, VERO cells were fixed with 4% paraformaldehyde (PFA, MilliporeSigma, MA) overnight and stained with 0.2% crystal violet. Plaques from each well were counted and neutralization % was calculated by using the formula: [(number of ZIKV plaque per well in virus only control wells)-(number of ZIKV plaque per well of diluted serum) / (number of ZIKV plaque per well in virus only control wells) x 100]. Neutralizing titers >10 refer to constructs with >50% neutralization at a 1:10 serum dilution.

Acknowledgements

This work was supported by funds provided by the School of Life Sciences, the Graduate and Professional Student Association, and the Center for Immunotherapy, Vaccines, and Virotherapy of the Biodesign Insitute at Arizona State University. This work was also supported in part by a grant from National Institute of Allergy and Infectious Diseases (NIAID) # R33AI101329 to QC.

Conflict of Interest

The authors have no conflicts of interest to declare.

Author Contributions

AD and HM designed experiments and analyzed data. AD, HM, and MP constructed vectors. AD performed C1q binding, solubility, sucrose gradient, and expression experiments. AD, JH, and MP performed purification experiments. AD and JH performed stability experiments. JK performed mouse immunization and bleeds. AD and MP performed antibody titer experiments. HS performed ZIKV neutralization experiments. AD wrote the manuscript. AD, HM, and QC critically revised the MS.

References

Akkaya, M., Kwak, K., and Pierce, S. K. (2020). B cell memory: building two walls of protection against pathogens. *Nat. Rev. Immunol.* 20, 229–238. doi:10.1038/s41577-019-0244-2.

Alam, A., Jiang, L., Kittleson, G. A., Steadman, K. D., Nandi, S., Fuqua, J. L., et al. (2018). Technoeconomic Modeling of Plant-Based Griffithsin Manufacturing. *Front. Bioeng. Biotechnol.* 6, 102. doi:10.3389/fbioe.2018.00102.

Bournazos, S., and Ravetch, J. V. (2017). Fcγ Receptor Function and the Design of Vaccination Strategies. *Immunity* 47, 224–233. doi:10.1016/j.immuni.2017.07.009.

Buyel, J. F. (2019). Plant molecular farming – Integration and exploitation of side streams to achieve sustainable biomanufacturing. *Front. Plant Sci.* 9. doi:10.3389/fpls.2018.01893.

Carter, P. J. (2011). Introduction to current and future protein therapeutics: A protein engineering perspective. *Exp. Cell Res.* 317, 1261–1269. doi:10.1016/j.yexcr.2011.02.013.

Castilho, A., and Steinkellner, H. (2012). Glyco-engineering in plants to produce human-like N-glycan structures. *Biotechnol. J.* 7, 1088–1098. doi:10.1002/biot.201200032.

Chargelegue, D., Drake, P. M. W., Obregon, P., Prada, A., Fairweather, N., and Ma, J. K. C. (2005). Highly immunogenic and protective recombinant vaccine candidate expressed in transgenic plants. *Infect. Immun.* 73, 5915–5922. doi:10.1128/IAI.73.9.5915-5922.2005.

Chen, Q., and Davis, K. R. (2016). The potential of plants as a system for the development and production of human biologics. *F1000Research* 5, 912. doi:10.12688/f1000research.8010.1.

Croix, D. A., Ahearn, J. M., Rosengard, A. M., Han, S., Kelsoe, G., Ma, M., et al. (1996). Antibody response to a T-dependent antigen requires B cell expression of complement

receptors. *J. Exp. Med.* 183, 1857–1864. doi:10.1084/jem.183.4.1857.

Czajkowsky, D. M., Hu, J., Shao, Z., and Pleass, R. J. (2012). Fc-fusion proteins: New developments and future perspectives. *EMBO Mol. Med.* 4, 1015–1028. doi:10.1002/emmm.201201379.

D'Eall, C., Pon, R. A., Rossotti, M. A., Krahn, N., Spearman, M., Callaghan, D., et al. (2019). Modulating antibody-dependent cellular cytotoxicity of epidermal growth factor receptor-specific heavy-chain antibodies through hinge engineering. *Immunol. Cell Biol.* doi:10.1111/imcb.12238.

Dekkers, G., Bentlage, A. E. H., Stegmann, T. C., Howie, H. L., Lissenberg-Thunnissen, S., Zimring, J., et al. (2017). Affinity of human IgG subclasses to mouse Fc gamma receptors. *MAbs* 9, 767–773. doi:10.1080/19420862.2017.1323159.

Dent, M., Hurtado, J., Paul, A. M., Sun, H., Lai, H., Yang, M., et al. (2016). Plant-produced anti-dengue virus monoclonal antibodies exhibit reduced antibody-dependent enhancement of infection activity. *J. Gen. Virol.* 97, 3280–3290. doi:10.1099/jgv.0.000635.

Diamos, A. G., Hunter, J. G. L., Pardhe, M. D., Rosenthal, S. H., Sun, H., Foster, B. C., et al. (2020a). High Level Production of Monoclonal Antibodies Using an Optimized Plant Expression System. *Front. Bioeng. Biotechnol.* 7, 472. doi:10.3389/fbioe.2019.00472.

Diamos, A. G., Larios, D., Brown, L., Kilbourne, J., Kim, H. S., Saxena, D., et al. (2019). Vaccine synergy with virus-like particle and immune complex platforms for delivery of human papillomavirus L2 antigen. *Vaccine* 37, 137–144. doi:10.1016/j.vaccine.2018.11.021.

Diamos, A. G., Pardhe, M. D., Sun, H., Hunter, J. G. L., Mor, T., Meador, L., et al. (2020b). Codelivery of improved immune complex and virus-like particle vaccines containing Zika

virus envelope domain III synergistically enhances immunogenicity. *Vaccine* 38, 3455–3463. doi:10.1016/j.vaccine.2020.02.089.

Diamos, A. G., Rosenthal, S. H., and Mason, H. S. (2016). 5' and 3' Untranslated Regions Strongly Enhance Performance of Geminiviral Replicons in Nicotiana benthamiana Leaves. *Front. Plant Sci.* 7, 200. doi:10.3389/fpls.2016.00200.

Diebolder, C. A., Beurskens, F. J., de Jong, R. N., Koning, R. I., Strumane, K., Lindorfer, M. A., et al. (2014). Complement Is Activated by IgG Hexamers Assembled at the Cell Surface. *Science (80-.).* 343, 1260–1263. doi:10.1126/science.1248943.

Fletcher, E. A. K., van Maren, W., Cordfunke, R., Dinkelaar, J., Codee, J. D. C., van der Marel, G., et al. (2018). Formation of Immune Complexes with a Tetanus-Derived B Cell Epitope Boosts Human T Cell Responses to Covalently Linked Peptides in an Ex Vivo Blood Loop System. *J. Immunol.* 201, 87–97. Available at: http://www.ncbi.nlm.nih.gov/pubmed/29752315 [Accessed May 28, 2019].

Forthal, D. N., Gach, J. S., Landucci, G., Jez, J., Strasser, R., Kunert, R., et al. (2010). Fc-Glycosylation Influences Fcγ Receptor Binding and Cell-Mediated Anti-HIV Activity of Monoclonal Antibody 2G12. *J. Immunol.* 185, 6876–6882. doi:10.4049/jimmunol.1002600.

Getahun, A., and Heyman, B. (2006). How antibodies act as natural adjuvants. *Immunol. Lett.* 104, 38–45. doi:10.1016/j.imlet.2005.11.005.

Gleba, Y. Y., Tusé, D., and Giritch, A. (2014). Plant viral vectors for delivery by Agrobacterium. *Curr. Top. Microbiol. Immunol.* 375, 155–92. doi:10.1007/82_2013_352.

Gupta, S. K., and Shukla, P. (2018). Glycosylation control technologies for recombinant therapeutic proteins. *Appl. Microbiol. Biotechnol.* 102, 10457–10468. doi:10.1007/s00253-

018-9430-6.

He, J., Lai, H., Engle, M., Gorlatov, S., Gruber, C., Steinkellner, H., et al. (2014). Generation and Analysis of Novel Plant-Derived Antibody-Based Therapeutic Molecules against West Nile Virus. *PLoS One* 9, e93541. doi:10.1371/journal.pone.0093541.

Heider, K.-H., Kiefer, K., Zenz, T., Volden, M., Stilgenbauer, S., Ostermann, E., et al. (2011). A novel Fc-engineered monoclonal antibody to CD37 with enhanced ADCC and high proapoptotic activity for treatment of B-cell malignancies. *Blood* 118, 4159–4168. doi:10.1182/blood-2011-04-351932.

Hioe, C. E., Kumar, R., Upadhyay, C., Jan, M., Fox, A., Itri, V., et al. (2018). Modulation of Antibody Responses to the V1V2 and V3 Regions of HIV-1 Envelope by Immune Complex Vaccines. *Front. Immunol.* 9, 2441. doi:10.3389/fimmu.2018.02441.

Ho, N. I., Camps, M. G. M., de Haas, E. F. E., Trouw, L. A., Verbeek, J. S., and Ossendorp, F. (2017). C1q-Dependent Dendritic Cell Cross-Presentation of In Vivo-Formed Antigen-Antibody Complexes. *J. Immunol.* 198, 4235–4243. doi:10.4049/jimmunol.1602169.

Huang, Z., and Mason, H. S. (2004). Conformational analysis of hepatitis B surface antigen fusions in an Agrobacterium-mediated transient expression system. *Plant Biotechnol. J.* 2, 241–9. doi:10.1111/j.1467-7652.2004.00068.x.

Huber, V. C., McKeon, R. M., Brackin, M. N., Miller, L. A., Keating, R., Brown, S. A., et al. (2006). Distinct contributions of vaccine-induced immunoglobulin G1 (IgG1) and IgG2a antibodies to protective immunity against influenza. *Clin. Vaccine Immunol.* 13, 981–990. doi:10.1128/CVI.00156-06.

Hurtado, J., Acharya, D., Lai, H., Sun, H., Kallolimath, S., Steinkellner, H., et al. (2019). In vitro

651 and in vivo efficacy of anti-chikungunya virus monoclonal antibodies produced in wild-type
652 and glycoengineered Nicotiana benthamiana plants. *Plant Biotechnol. J.*
653 doi:10.1111/pbi.13194.

654 Kallolimath, S., and Steinkellner, H. (2015). Glycosylation of plant produced human antibodies.
655 *Hum. Antibodies* 23, 45–48. doi:10.3233/HAB-150283.

656 Kim, M.-Y., Reljic, R., Kilbourne, J., Ceballos-Olvera, I., Yang, M.-S., Reyes-del Valle, J., et al.
657 (2015). Novel vaccination approach for dengue infection based on recombinant immune
658 complex universal platform. *Vaccine* 33, 1830–1838. doi:10.1016/j.vaccine.2015.02.036.

659 Kim, M. Y., Copland, A., Nayak, K., Chandele, A., Ahmed, M. S., Zhang, Q., et al. (2018).
660 Plant-expressed Fc-fusion protein tetravalent dengue vaccine with inherent adjuvant
661 properties. *Plant Biotechnol. J.* 16, 1283–1294. doi:10.1111/pbi.12869.

662 Konduru, K., Bradfute, S. B., Jacques, J., Manangeeswaran, M., Nakamura, S., Morshed, S., et al.
663 (2011). Ebola virus glycoprotein Fc fusion protein confers protection against lethal
664 challenge in vaccinated mice. *Vaccine* 29, 2968–2977. doi:10.1016/j.vaccine.2011.01.113.

665 Lagassé, H. A. D., Hengel, H., Golding, B., and Sauna, Z. E. (2019). Fc-Fusion Drugs Have
666 FcγR/C1q Binding and Signaling Properties That May Affect Their Immunogenicity. *AAPS*
667 *J.* 21, 62. doi:10.1208/s12248-019-0336-8.

668 Lazar, G. A., Dang, W., Karki, S., Vafa, O., Peng, J. S., Hyun, L., et al. (2006). Engineered
669 antibody Fc variants with enhanced effector function. *Proc. Natl. Acad. Sci. U. S. A.* 103,
670 4005–10. doi:10.1073/pnas.0508123103.

671 Loureiro, S., Ren, J., Phapugrangkul, P., Colaco, C. A., Bailey, C. R., Shelton, H., et al. (2011).
672 Adjuvant-Free Immunization with Hemagglutinin-Fc Fusion Proteins as an Approach to

673 Influenza Vaccines. *J. Virol.* 85, 3010–3014. doi:10.1128/jvi.01241-10.

674 Lu, L. L., Suscovich, T. J., Fortune, S. M., and Alter, G. (2018). Beyond binding: Antibody
675 effector functions in infectious diseases. *Nat. Rev. Immunol.* 18, 46–61.
676 doi:10.1038/nri.2017.106.

677 Lyon, G. M., Mehta, A. K., Varkey, J. B., Brantly, K., Plyler, L., McElroy, A. K., et al. (2014).
678 Clinical care of two patients with Ebola virus disease in the United States. *N. Engl. J. Med.*
679 371, 2402–9. doi:10.1056/NEJMoa1409838.

680 Ma, J. K. C., Christou, P., Chikwamba, R., Haydon, H., Paul, M., Ferrer, M. P., et al. (2013).
681 Realising the value of plant molecular pharming to benefit the poor in developing countries
682 and emerging economies. *Plant Biotechnol. J.* 11, 1029–1033. doi:10.1111/pbi.12127.

683 Marusic, C., Pioli, C., Stelter, S., Novelli, F., Lonoce, C., Morrocchi, E., et al. (2018). N-glycan
684 engineering of a plant-produced anti-CD20-hIL-2 immunocytokine significantly enhances
685 its effector functions. *Biotechnol. Bioeng.* 115, 565–576. doi:10.1002/bit.26503.

686 Mason, H. S. (2016). Recombinant immune complexes as versatile and potent vaccines. *Hum.*
687 *Vaccin. Immunother.* 12, 988–9. doi:10.1080/21645515.2015.1116655.

688 Mastrangeli, R., Palinsky, W., and Bierau, H. (2019). Glycoengineered antibodies: towards the
689 next-generation of immunotherapeutics. *Glycobiology* 29, 199–210.
690 doi:10.1093/glycob/cwy092.

691 McCloskey, M. L., Curotto De Lafaille, M. A., Carroll, M. C., and Erlebacher, A. (2011).
692 Acquisition and presentation of follicular dendritic cell-bound antigen by lymph node-
693 resident dendritic cells. *J. Exp. Med.* 208, 135–148. doi:10.1084/jem.20100354.

694 Olinger, G. G., Pettitt, J., Kim, D., Working, C., Bohorov, O., Bratcher, B., et al. (2012).

695 Delayed treatment of Ebola virus infection with plant-derived monoclonal antibodies
696 provides protection in rhesus macaques. *Proc. Natl. Acad. Sci. U. S. A.* 109, 18030–5.
697 doi:10.1073/pnas.1213709109.

698 Pepponi, I., Diogo, G. R., Stylianou, E., van Dolleweerd, C. J., Drake, P. M. W., Paul, M. J., et al.
699 (2014). Plant-derived recombinant immune complexes as self-adjuvanting TB immunogens
700 for mucosal boosting of BCG. *Plant Biotechnol. J.* 12, 840–850. doi:10.1111/pbi.12185.

701 Phan, T. G., Grigorova, I., Okada, T., and Cyster, J. G. (2007). Subcapsular encounter and
702 complement-dependent transport of immune complexes by lymph node B cells. *Nat.*
703 *Immunol.* 8, 992–1000. doi:10.1038/ni1494.

704 Phoolcharoen, W., Bhoo, S. H., Lai, H., Ma, J., Arntzen, C. J., Chen, Q., et al. (2011a).
705 Expression of an immunogenic Ebola immune complex in Nicotiana benthamiana. *Plant*
706 *Biotechnol. J.* 9, 807–16. doi:10.1111/j.1467-7652.2011.00593.x.

707 Phoolcharoen, W., Dye, J. M., Kilbourne, J., Piensook, K., Pratt, W. D., Arntzen, C. J., et al.
708 (2011b). A nonreplicating subunit vaccine protects mice against lethal Ebola virus challenge.
709 *Proc. Natl. Acad. Sci. U. S. A.* 108, 20695–700. doi:10.1073/pnas.1117715108.

710 Qiu, X., Wong, G., Audet, J., Bello, A., Fernando, L., Alimonti, J. B., et al. (2014). Reversion of
711 advanced Ebola virus disease in nonhuman primates with ZMapp. *Nature* 514, 47–53.
712 doi:10.1038/nature13777.

713 Reed, S. G., Orr, M. T., and Fox, C. B. (2013). Key roles of adjuvants in modern vaccines. *Nat.*
714 *Med.* 19, 1597–1608. doi:10.1038/nm.3409.

715 Robbie, G. J., Criste, R., Dall'acqua, W. F., Jensen, K., Patel, N. K., Losonsky, G. A., et al.
716 (2013). A novel investigational Fc-modified humanized monoclonal antibody,

motavizumab-YTE, has an extended half-life in healthy adults. *Antimicrob. Agents Chemother.* 57, 6147–53. doi:10.1128/AAC.01285-13.

Roopenian, D. C., and Akilesh, S. (2007). FcRn: the neonatal Fc receptor comes of age. *Nat. Rev. Immunol.* 7, 715–725. doi:10.1038/nri2155.

Santi, L., Batchelor, L., Huang, Z., Hjelm, B., Kilbourne, J., Arntzen, C. J., et al. (2008). An efficient plant viral expression system generating orally immunogenic Norwalk virus-like particles. *Vaccine* 26, 1846–54. doi:10.1016/j.vaccine.2008.01.053.

Strasser, R., Stadlmann, J., Schähs, M., Stiegler, G., Quendler, H., Mach, L., et al. (2008). Generation of glyco-engineered Nicotiana benthamiana for the production of monoclonal antibodies with a homogeneous human-like N-glycan structure. *Plant Biotechnol. J.* 6, 392–402. doi:10.1111/j.1467-7652.2008.00330.x.

Sun, H., Chen, Q., and Lai, H. (2018). Development of antibody therapeutics against flaviviruses. *Int. J. Mol. Sci.* 19. doi:10.3390/ijms19010054.

Tsouchnikas, G., Zlatkovic, J., Jarmer, J., Strauß, J., Vratskikh, O., Kundi, M., et al. (2015). Immunization with Immune Complexes Modulates the Fine Specificity of Antibody Responses to a Flavivirus Antigen. *J. Virol.* 89, 7970–8. doi:10.1128/JVI.00938-15.

van Montfoort, N., Mangsbo, S. M., Camps, M. G. M., van Maren, W. W. C., Verhaart, I. E. C., Waisman, A., et al. (2012). Circulating specific antibodies enhance systemic cross-priming by delivery of complexed antigen to dendritic cells in vivo. *Eur. J. Immunol.* 42, 598–606. doi:10.1002/eji.201141613.

Wang, G., de Jong, R. N., van den Bremer, E. T. J., Beurskens, F. J., Labrijn, A. F., Ugurlar, D., et al. (2016). Molecular Basis of Assembly and Activation of Complement Component C1

in Complex with Immunoglobulin G1 and Antigen. *Mol. Cell* 63, 135–145. doi:10.1016/J.MOLCEL.2016.05.016.

Wang, Q., Chung, C.-Y., Chough, S., and Betenbaugh, M. J. (2018). Antibody glycoengineering strategies in mammalian cells. *Biotechnol. Bioeng.* 115, 1378–1393. doi:10.1002/bit.26567.

Webster, G. R., van Dolleweerd, C., Guerra, T., Stelter, S., Hofmann, S., Kim, M. Y., et al. (2018). A polymeric immunoglobulin—antigen fusion protein strategy for enhancing vaccine immunogenicity. *Plant Biotechnol. J.* 16, 1983–1996. doi:10.1111/pbi.12932.

West, E. E., Kolev, M., and Kemper, C. (2018). Complement and the Regulation of T Cell Responses. *Annu. Rev. Immunol.* 36, 309–338. doi:10.1146/annurev-immunol-042617-053245.

Wilson, J. A., Hevey, M., Bakken, R., Guest, S., Bray, M., Schmaljohn, A. L., et al. (2000). Epitopes involved in antibody-mediated protection from Ebola virus. *Science* 287, 1664–6. Available at: http://www.ncbi.nlm.nih.gov/pubmed/10698744 [Accessed June 15, 2019].

Yan, B., Boyd, D., Kaschak, T., Tsukuda, J., Shen, A., Lin, Y., et al. (2012). Engineering Upper Hinge Improves Stability and Effector Function of a Human IgG1. *J. Biol. Chem.* 287, 5891–5897. doi:10.1074/jbc.M111.311811.

Yang, M., Dent, M., Lai, H., Sun, H., and Chen, Q. (2017). Immunization of Zika virus envelope protein domain III induces specific and neutralizing immune responses against Zika virus. *Vaccine* 35, 4287–4294. doi:10.1016/j.vaccine.2017.04.052.

Zeitlin, L., Pettitt, J., Scully, C., Bohorova, N., Kim, D., Pauly, M., et al. (2011). Enhanced potency of a fucose-free monoclonal antibody being developed as an Ebola virus immunoprotectant. *Proc. Natl. Acad. Sci.* 108, 20690–20694. doi:10.1073/pnas.1108360108.

761 Zeng, F., Yang, C., Gao, X., Li, X., Zhang, Z., and Gong, R. (2018). Comprehensive elucidation
762 of the structural and functional roles of engineered disulfide bonds in antibody Fc fragment.
763 *J. Biol. Chem.* 293, 19127–19135. doi:10.1074/jbc.RA118.005367.

764 Zhang, D., Armstrong, A. A., Tam, S. H., McCarthy, S. G., Luo, J., Gilliland, G. L., et al. (2017).
765 Functional optimization of agonistic antibodies to OX40 receptor with novel Fc mutations
766 to promote antibody multimerization. *MAbs* 9, 1129–1142.
767 doi:10.1080/19420862.2017.1358838.

768 Zhang, Y., Zhou, Z., Zhu, S. L., Zu, X., Wang, Z., Zhang, L. ke, et al. (2019). A novel RSV F-Fc
769 fusion protein vaccine reduces lung injury induced by respiratory syncytial virus infection.
770 *Antiviral Res.* 165, 11–22. doi:10.1016/j.antiviral.2019.02.017.

771 Zhao, B., Zhang, X., Krummenacher, C., Song, S., Gao, L., Zhang, H., et al. (2018).
772 Immunization with Fc-based recombinant Epstein-Barr virus gp350 elicits potent
773 neutralizing humoral immune response in a BALB/c mice model. *Front. Immunol.* 9, 932.
774 doi:10.3389/fimmu.2018.00932.

775

776

Supporting Info

Figure S1. C1q binding comparison between wildtype and glycoengineered plants

Figure S2. C1q binding comparison between IgG fusions

Figure S3. Epitope binding of single chain 6D8

Figure S4. RIC insolubility

Figure S5. Solubility and binding of 6D8 epitope tag mutants

Tables

Construct	Expression	Solubility	Sedimentation	Stability	C1q	IgG	IgG2a	Neutralization
ZE3	N.D.	N.D.	N.D.	N.D.	N.D.	+	+	++
HLZ	0.17 mg/g	High	+	Medium	+	+++	++	+++
HLZe	0.22 mg/g	Low	++++	High	++	+++	++	+++
HLZd	1.50 mg/g	High	++	High	+++	+++	+++	+++
ZH	0.83 mg/g	High	+	Medium	++	+++	+++	+++
ZHx	0.21 mg/g	Low	+++*	High	+++	+++	+++	+++
VHLZe	<0.1 mg/g	Low	++++	High	+++	+++	+++	+++
ZFc	0.57 mg/g	High	+	Low	+++	+++	+++	+++

Table 1. Summary of characteristics of IgG fusions

A summary of the characteristics of each IgG fusion vaccine candidate is given. For expression, only the yield (mg/g LFW) of the fully assembled product is shown. A greater number of "+" symbols indicates either a statistically significant increase in the mean value for that property (for C1q, IgG, IgG2a, and neutralization), or a repeatably observed difference (for sedimentation). For ZHx (*), peaks of both low- and high-velocity sedimentation were observed.

Figure Legends

Figure 1. Various IgG fusion strategies enhance C1q binding

(A) Schematic representation of IgG fusion constructs used in this study. Fusion constructs are built on the mAb 6D8 human IgG1 backbone with the shown modifications. ZE3; the Zika envelope domain III containing amino acids K301 to T406; e, an epitope tag containing the "VYKLDISEA" 6D8 binding motif for RIC formation; e with lightning bolt, an epitope tag truncated to include only "YKLDIS" to reduce RIC formation; VH, the variable heavy domain from 6D8 which participates in binding the epitope tag; VL, the variably light domain from 6D8 which participates in binding the epitope tag; H, the heavy chain constant CH1 domain from 6D8; L, the light chain constant domain from 6D8; Fc, the heavy chain constant CH2 or CH3 domains from 6D8; Fc with lightning bolt, same as Fc but with E345R, E430G, and S440Y mutations to induce hexamer formation. (B) C1q binding ELISA of purified IgG fusion constructs. ELISA plates were coated with 10 μg/ml human C1q and incubated with 10 μg/ml each molecule, using 6D8 with no fusion as a negative control. Constructs were detected using polyclonal goat anti-human IgG-HRP. Mean OD_{450} values from three samples are shown ± standard error with one star (*) indicating $p < 0.05$ and three stars (***) indicating $p < 0.001$ as measured by one-way ANOVA with comparisons between the indicated groups.

Figure 2. Modified IgG fusions have improved expression and solubility

(A) ELISA and gel quantification of IgG fusion construct expression. Clarified protein extracts ("soluble" fraction) from leaf spots agroinfiltrated with each IgG fusion construct were analyzed by either ELISA, or SDS-PAGE followed by gel image quantification. For ZE3 ELISA, plates were coated with polyclonal mouse anti-ZE3, incubated with serial dilutions of extracts from each IgG fusion using purified HLZ as a standard, and probed with goat anti-human IgG-HRP.

For IgG ELISA, plates were coated with serial dilutions of extracts or human IgG standard and probed with goat anti-human IgG-HRP. For gel quantification, ImageJ software was used to compare the IgG fusion band intensity visualized on stain-free polyacrylamide gels using purified 6D8 antibody as standard. Columns represent means ± standard error from three independently infiltrated leaf samples. (B) Clarified leaf extracts were separated by reducing SDS-PAGE and a representative gel image is shown. The band position corresponding to each respective heavy chain/ZE3 fusion is indicated "ZH/HZ." The small shift in size in HLZe and HLZd is due to epitope tag truncation. The "-" indicates ZE3-Fc and Fc fragments. The large subunit of Rubisco "RbcL."

Figure 3. Purification of IgG Fusions

Agroinfiltrated leaf material from between 1-3 plants per construct was homogenized, clarified, and purified by protein G affinity chromatography. The peak elutions were pooled and separated on nonreducing (NR) and reducing (R) SDS-PAGE using stain-free polyacrylamide gels. Representative lanes for each construct are compiled from multiple gels here.

Figure 4. Sucrose gradient centrifugation of IgG fusions

Purified IgG fusions were separated by sucrose gradient sedimentation using 5/10/15/20/25% discontinuous sucrose layers. Gradient fractions were analyzed by SDS-PAGE and representative results are shown; direction of sedimentation is left to right. The relative band intensity was quantified using ImageJ software and the peak band was arbitrarily assigned the value of 1.

Figure 5. Stability and C1q binding of purified IgG fusions

Samples of purified IgG fusions were frozen and thawed once after purification (initial), or additionally subjected to either additional 5 freeze/thaw cycles, incubation for 2 weeks at 4°C, or

837 incubation for 2 weeks at 23˚C. (A) After each treatment, samples were separated on reducing
838 and nonreducing SDS-PAGE gels, and the relative proportion of fully assembled product was
839 analyzed using ImageJ software. The initial measurement reflects degradation which occurred
840 during expression or purification, whereas the other measurements reflect degradation which
841 occurred during each respective treatment. (B) Samples from each treatment were analyzed by
842 C1q binding ELISA. Columns represent the mean OD_{450} value ± standard error from three
843 samples.

844 **Figure 6. Mouse immunization and serum titers**

845 BALB/c mice (6 per group) were immunized twice two weeks apart subcutaneously with a dose
846 that would deliver 8 μg ZE3 for each IgG fusion or with PBS as a control. Mouse serum samples
847 were collected two weeks after the final dose. (A) Serially diluted mouse serum was analyzed for
848 total IgG production by ELISA. The endpoint was taken as the reciprocal of the greatest dilution
849 that gave an OD_{450} reading at least twice the background. Three stars (***) indicates $p < 0.01$ by
850 one-way ANOVA comparing the indicated columns to ZE3. (B) Mouse serum samples were
851 diluted 1:100 and analyzed for IgG2a production by ELISA. (**) indicates $p < 0.05$ and (***)
852 indicates $p < 0.01$ by one-way ANOVA comparing the indicated columns to HLZ.

853 **Figure 7. Neutralization of ZIKV**

854 Plaque reduction neutralization assays (PRNT) assays were performed using pooled mouse sera
855 with dilution ratio of 1:10 to evaluate ZIKV-specific neutralizing antibodies in the sera. Data are
856 presented as mean neutralization % and SD from three independent experiments with technical
857 triplicates for each sample. Statistical analyses were performed using one-way ANOVA, p values
858 from comparison between vaccine treatments and PBS were indicated with **** (<0.0001) or

859 from comparison between vaccine treatments and His-tagged ZE3 were indicated with * ($p <$

860 0.024).

A

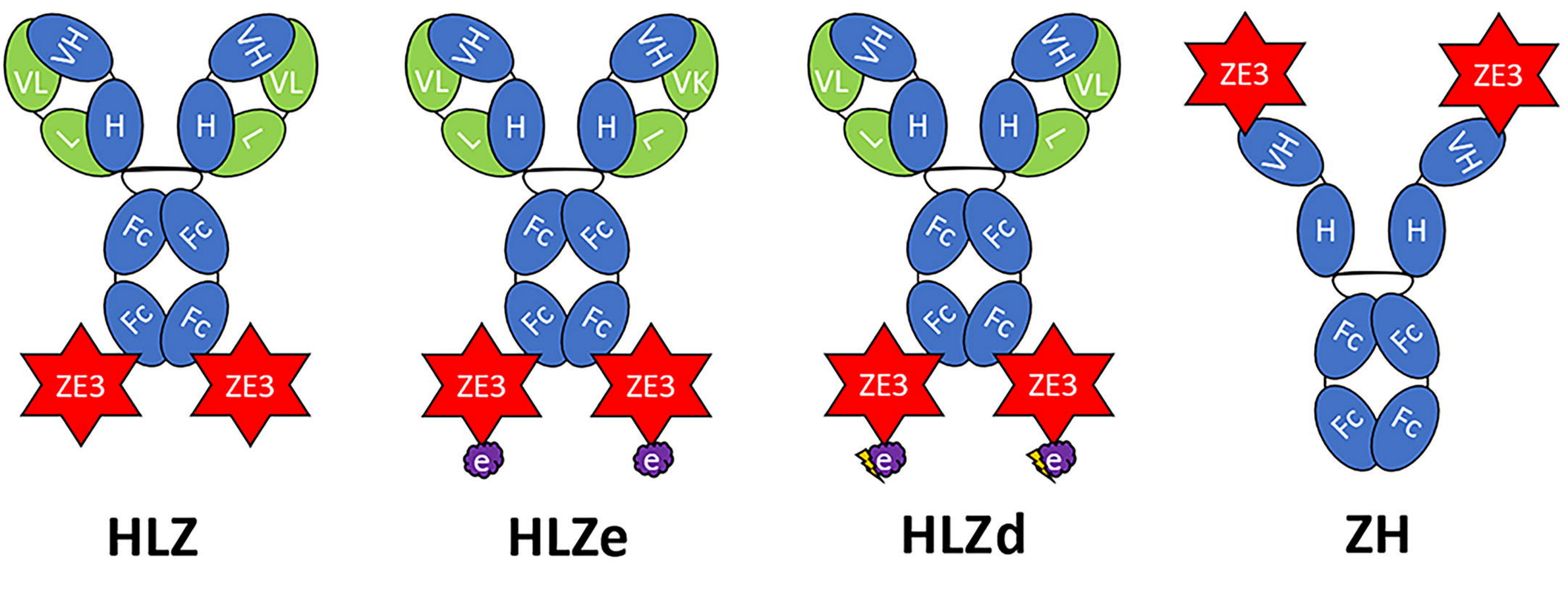

B

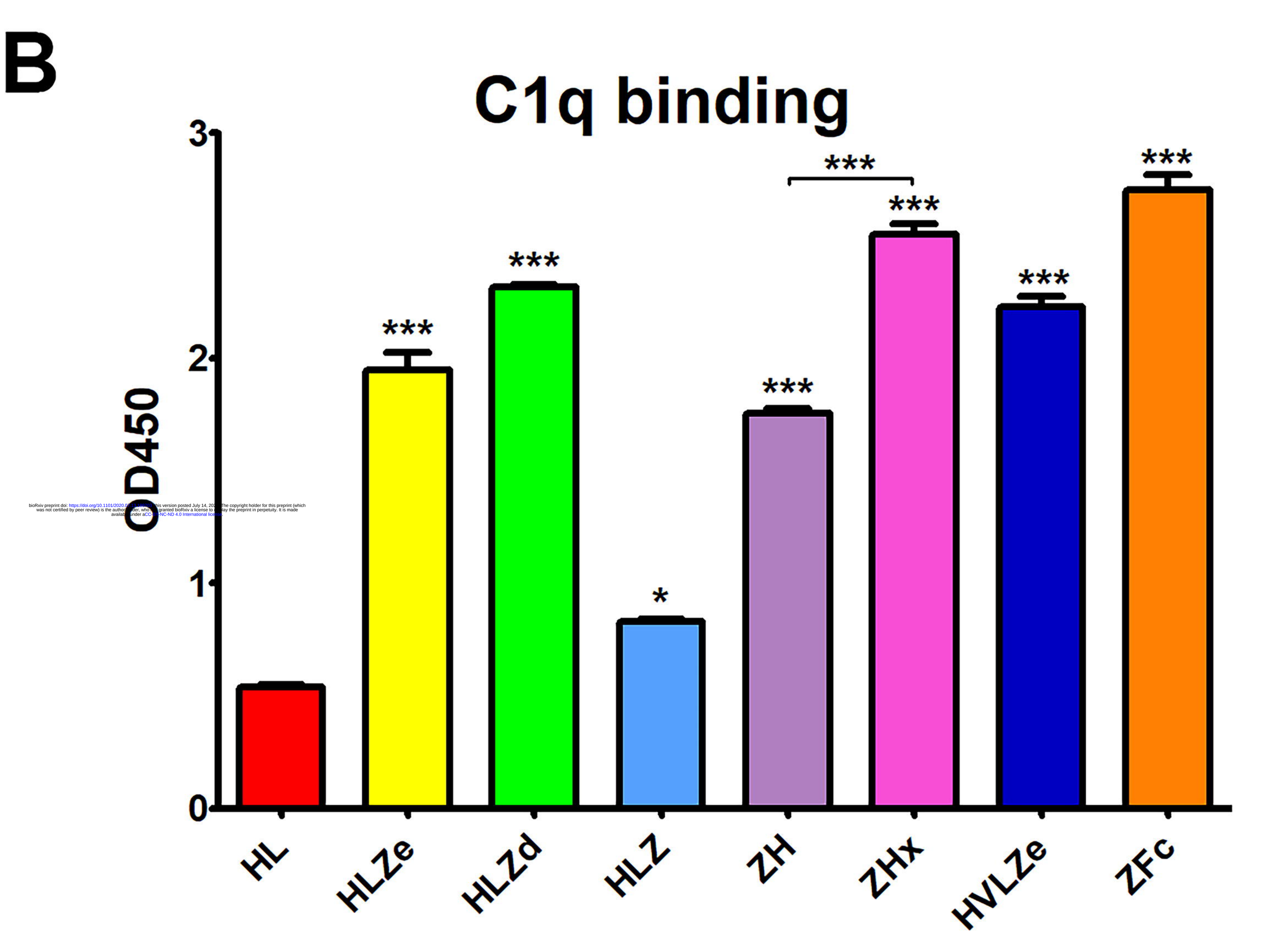

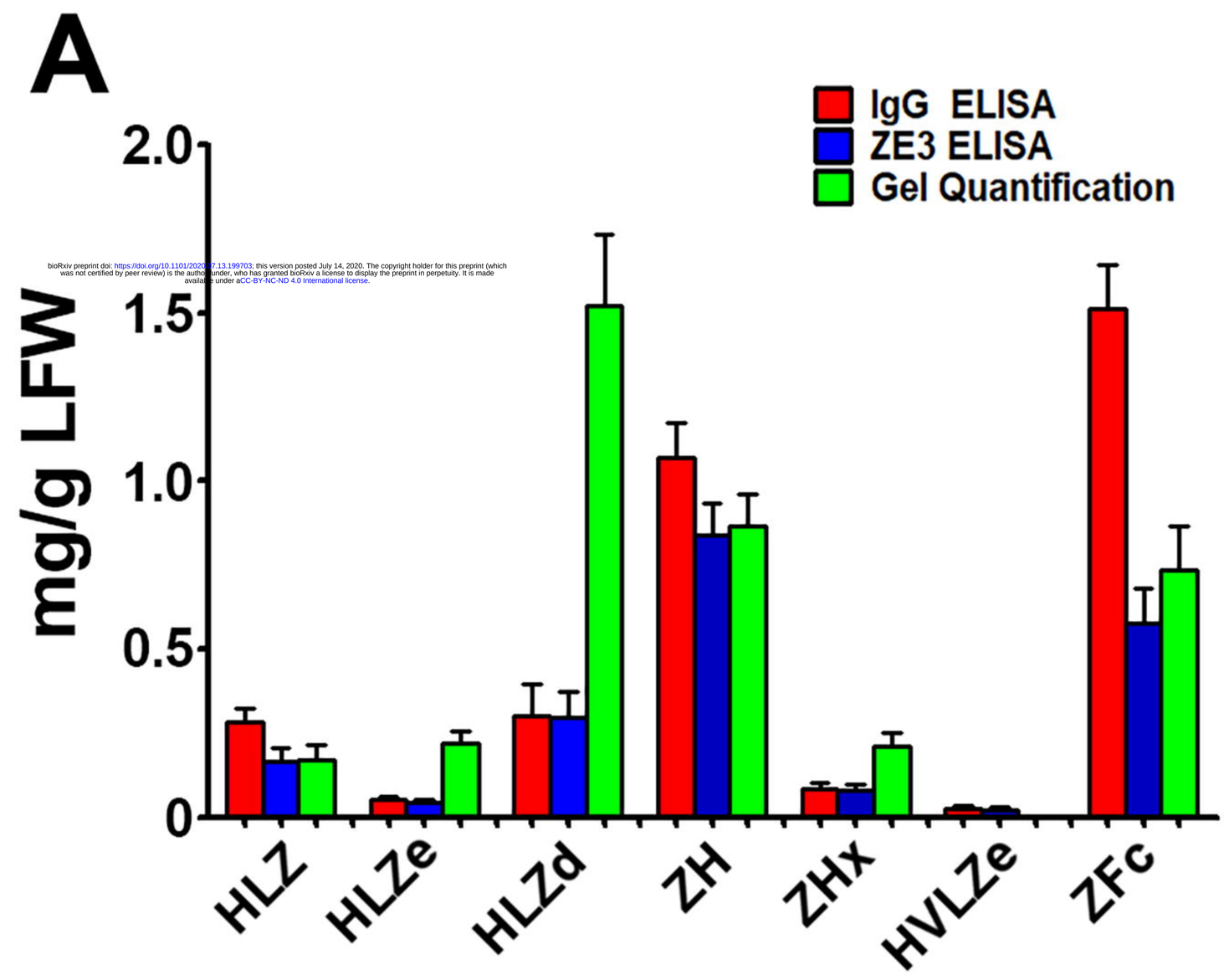

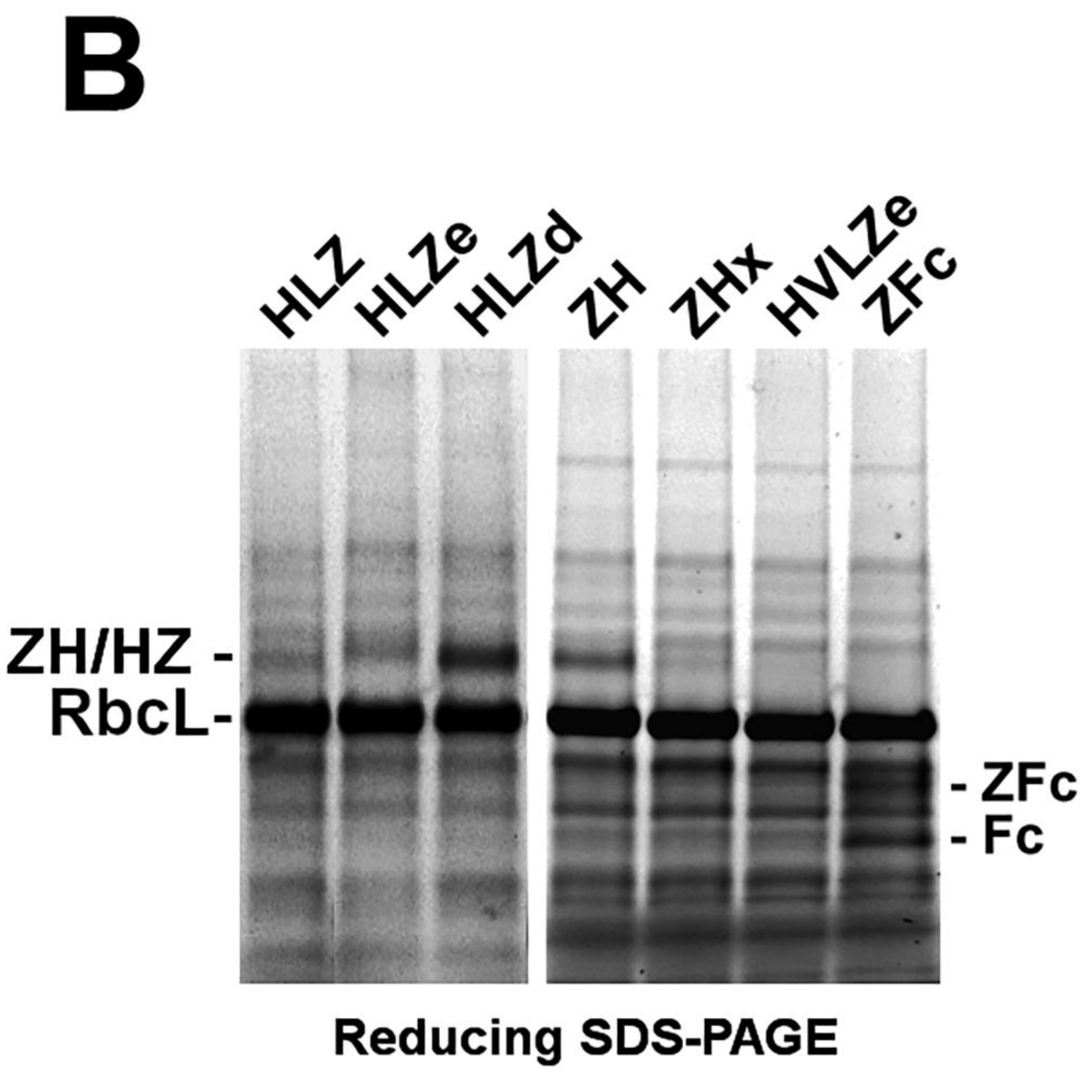

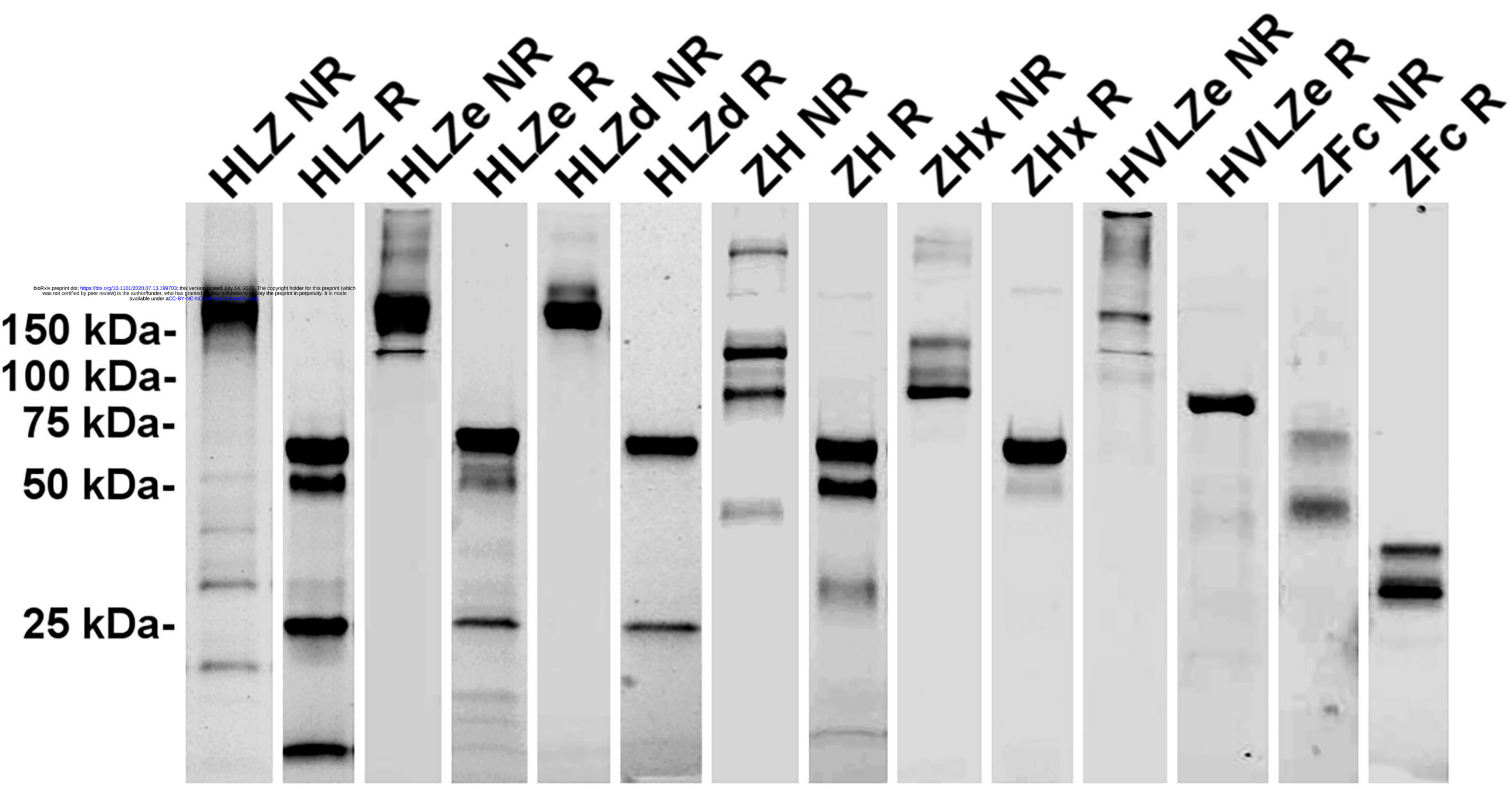

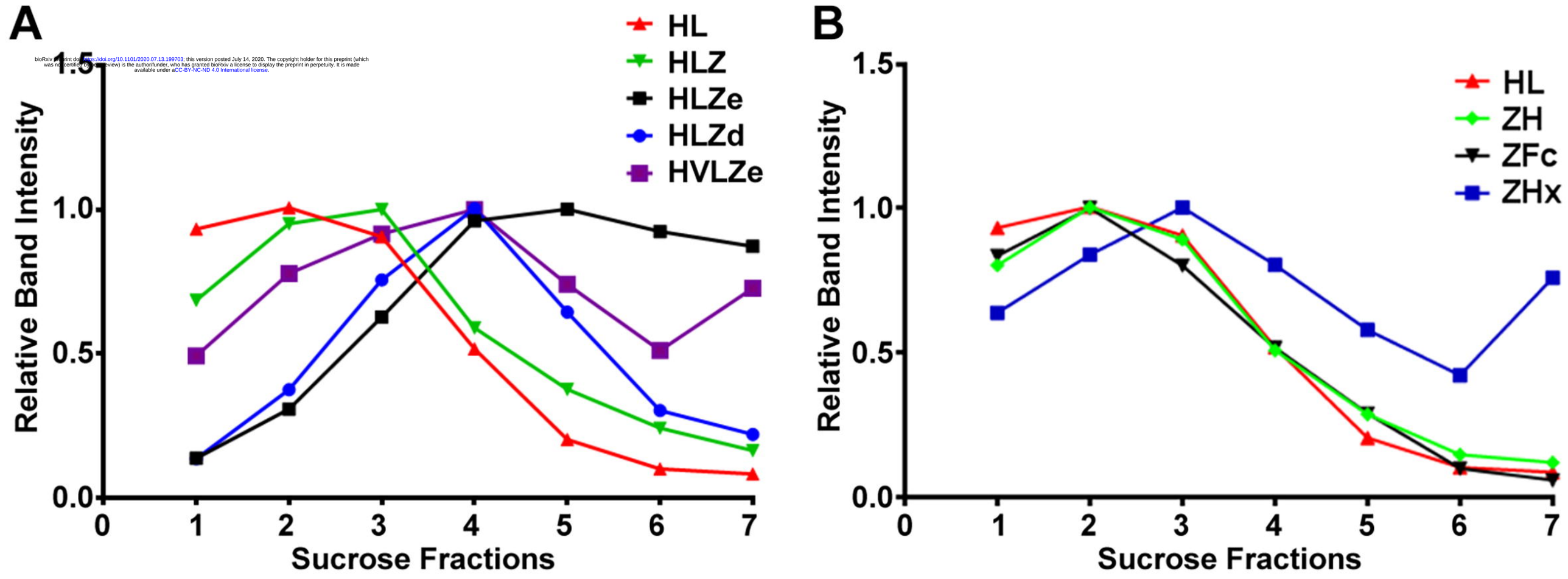

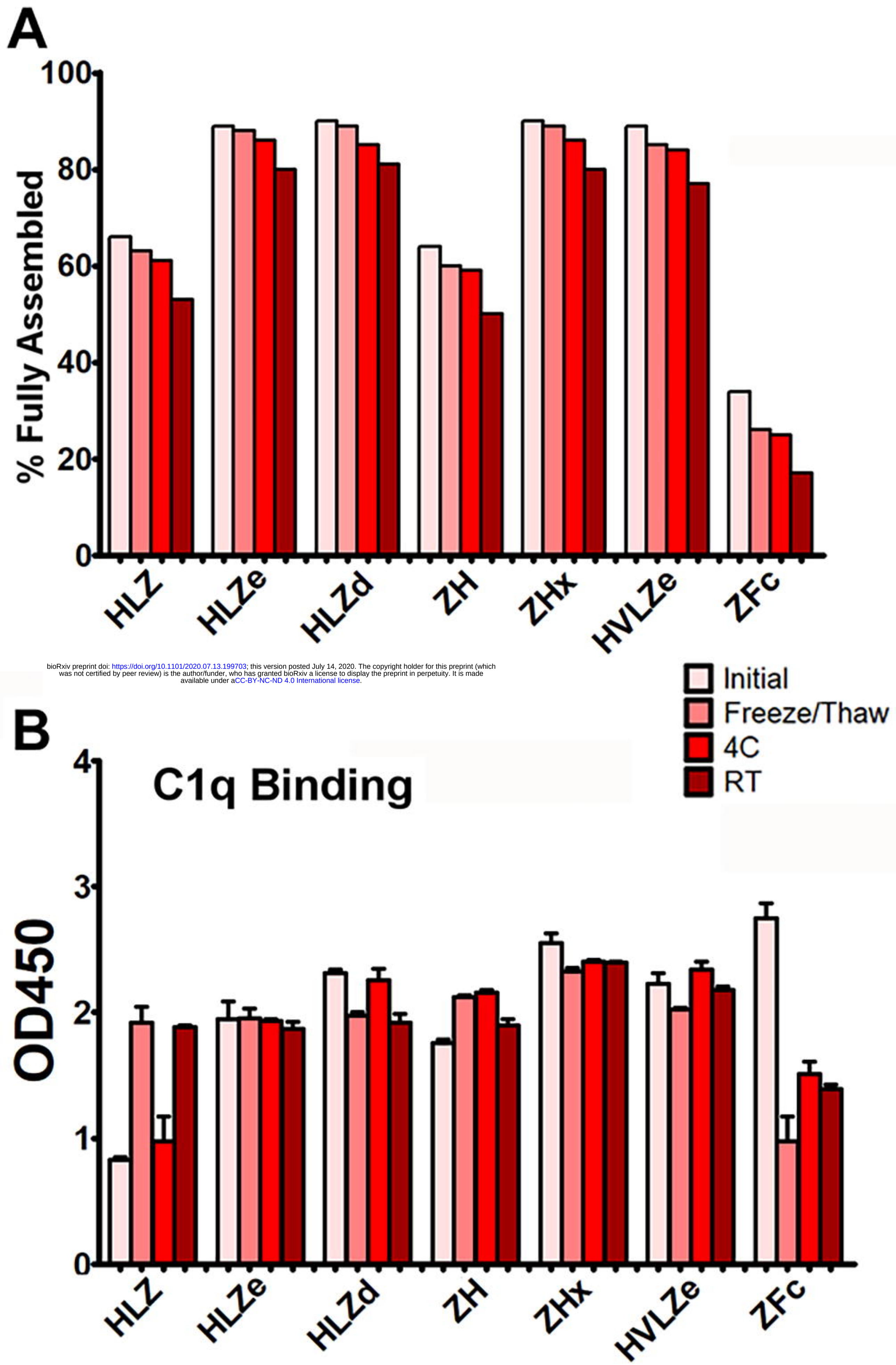

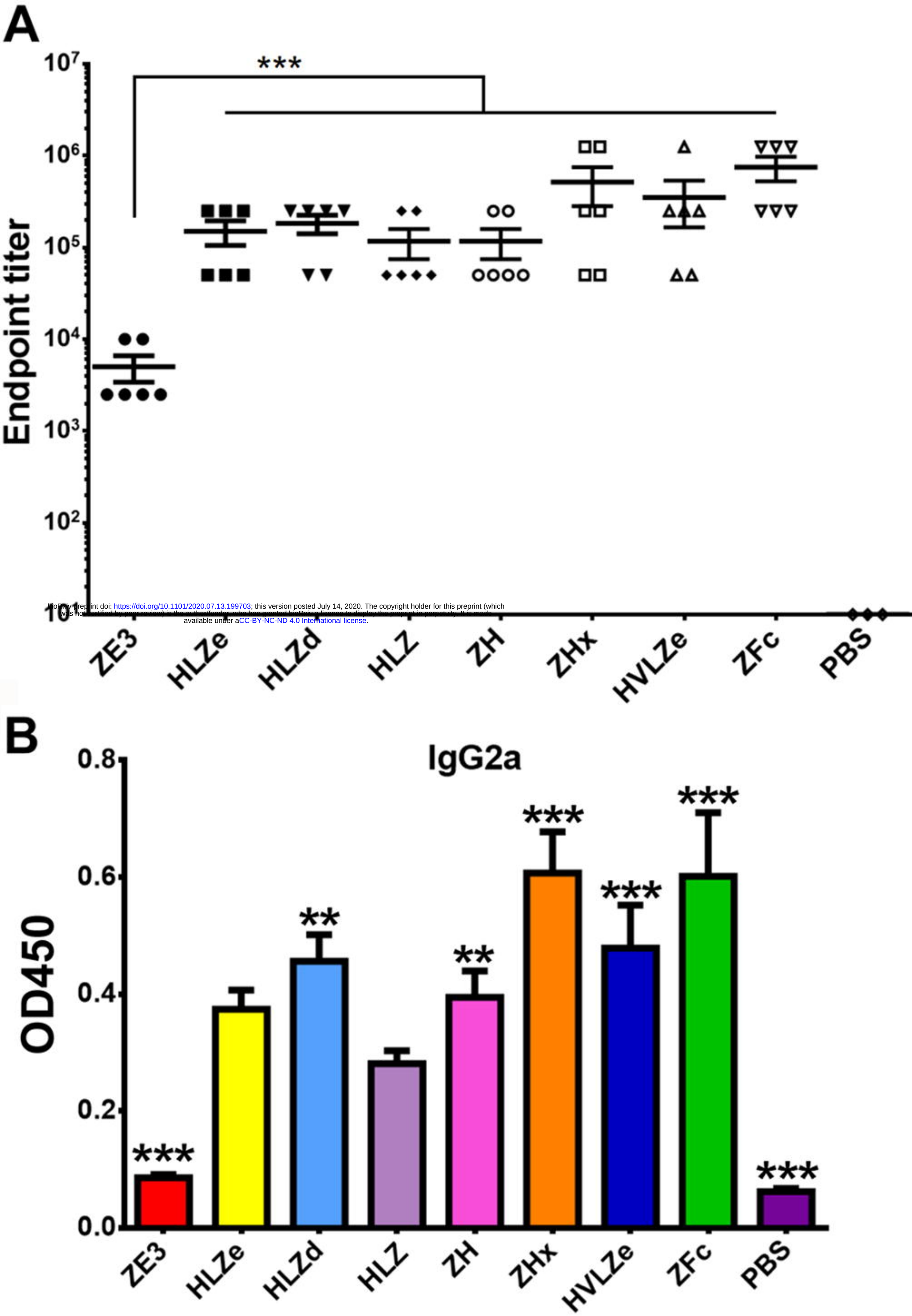

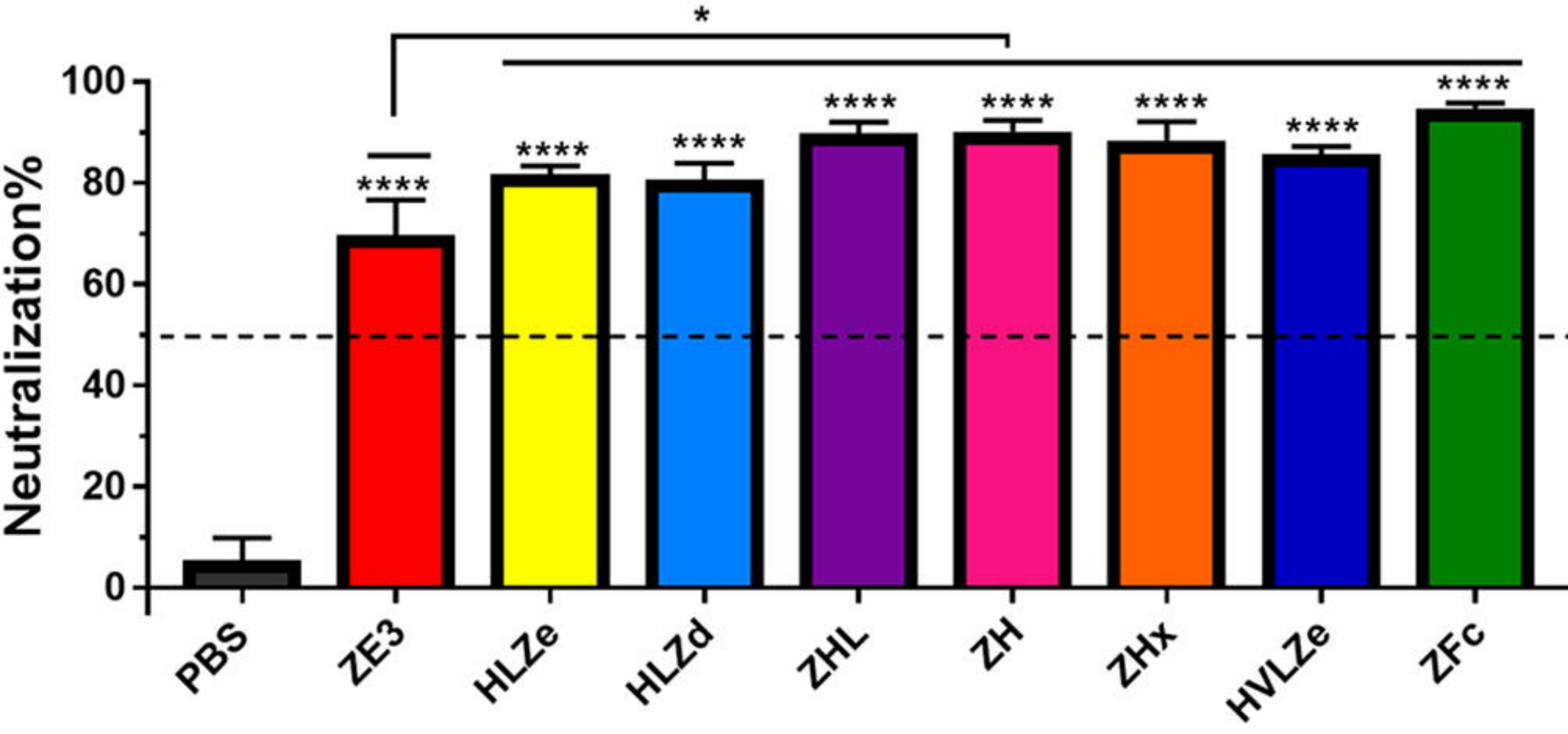
*
100
80
60
40
20
0
Neutralization%
****
****
****
****
****
****
****
PBS
ZE3
HLZe
HLZd
ZHL
ZH
ZHx
HVLZe
ZFc